Computers and Geotechnics 199 (2026) 108407

Contents lists available at ScienceDirect

Computers and Geotechnics

journal homepage: www.elsevier.com/locate/compgeo

Research paper

A general FEM framework for sedimentation and consolidation of diluted clay suspensions

Ismail Myouri *, Claire Chassagne

Delft University of Technology, Faculty of Civil Engineering and Geosciences, Environmental Fluid Mechanics, Box 5048, 2600 GA, Delft, The Netherlands

ARTICLE INFO

Keywords:
Sedimentation
Self-weight consolidation
Soft clay
Advection–diffusion model
Large strain
Finite element method
Hydraulic dredging
Land reclamation
Drainage

ABSTRACT

Soft fine-grained sediments placed by hydraulic dredging usually pass through two main stages: an initial sedimentation stage, where particles settle in suspension, and a later self-weight consolidation stage, where interparticle contacts develop and pore water is progressively expelled. In engineering practice, these two stages are often treated separately, which makes it difficult to describe the full evolution of very soft deposits within a single consistent model. This paper presents a unified finite element framework for sedimentation and consolidation of diluted clay suspensions. The formulation is based on a common set of governing equations and constitutive relations, allowing both regimes to be described within one continuous advection–diffusion framework. A smooth transition around the gelling concentration is introduced to avoid a discontinuous switch between sedimentation and consolidation, and a SUPG stabilization is used for advection-dominated transport. The model is applied to kaolinite K1 and Marker Wadden mud, and the results are compared with experimental measurements of interface evolution, density profiles, and drainage-induced settlement. The framework reproduces the main trends observed in both one-dimensional settling columns and drainage-controlled configurations. In addition, the formulation is compared with a large-strain finite element reference model using logarithmic compressibility, showing that the proposed approach remains consistent with more advanced hydro-mechanical descriptions while retaining a simpler constitutive structure that avoids tensorial stress updates, return-mapping algorithms, and additional internal variables. The proposed framework provides a practical tool for analyzing the evolution of very soft sediments from suspension to consolidated soil in geotechnical and land reclamation applications.

1. Introduction

The increasing demand for sustainable land development and the growing scarcity of high-quality sand resources are reshaping geotechnical practice in land reclamation. In many modern projects, fine dredged sediments are transported and placed using hydraulic dredging methods, in which the material is pumped as a highly diluted slurry with very high water content (Van Rijn, 2019; Miedema, 2006; Barciela-Rial et al., 2024b). Upon deposition, these suspensions behave initially as dilute particulate systems, where particle motion is governed by sedimentation processes rather than soil-mechanical consolidation. Only after sufficient densification do interparticle contacts develop and the material transitions into a self-weight consolidation regime. This operational practice implies that land-reclamation fills constructed with hydraulically dredged fines inevitably experience a sedimentation phase prior to consolidation.

The consolidation process is often accelerated through soil-optimization techniques such as staged loading, surcharge application, and installation of drainage systems (e.g., prefabricated vertical drains), which enhance pore-pressure dissipation and facilitate effective stress development (Chu and Varaksin, 2000; Moseley and Kirsch, 2004). The efficiency of these measures, however, strongly depends on the evolving material state, as permeability, compressibility, and density distribution vary significantly during consolidation and directly control pore-pressure dissipation and drainage efficiency (Indraratna et al., 2017; Mesri and Olson, 1997; Been and Sills, 1981; Winterwerp, 2002). Accurately predicting the full evolution of such deposits — from dilute suspension through gelling to large-strain consolidation, and ultimately to improved ground conditions — is therefore essential for reliable settlement prediction, production planning, and safe construction. Yet, a unified framework consistently linking sedimentation, consolidation, and optimization strategies remains largely absent in current engineering models.

When fine sediments are deposited hydraulically, they initially exist as highly diluted suspensions. In this stage, particles settle under gravity and their motion is governed by viscous drag and interparticle forces

* Corresponding author.
E-mail address: imyouri@tudelft.nl (I. Myouri).

https://doi.org/10.1016/j.compgeo.2026.108407
Received 20 April 2026; Received in revised form 10 June 2026; Accepted 1 July 2026
Available online 8 July 2026
0266-352X/

such as Brownian motion and electrostatic interactions (Richardson and Zaki, 1997; Winterwerp, 2002; Russel et al., 1991). Classical sedimentation theory, beginning with Kynch (1952), describes this regime by relating the settling velocity to the local particle concentration, assuming that effective stress is absent and the suspension behaves as a fluid. As settling proceeds, the solids concentration increases and particles begin to form a connected network. Once this network develops, effective stress becomes measurable and the material no longer behaves as a purely fluidic suspension. The process gradually transitions into self-weight consolidation, where deformation is controlled by contact forces within the solid skeleton and pore water is expelled through Darcy-type flow.

The theoretical relationship between sedimentation and consolidation has been clarified by several authors. Pane and Schiffman (1985) showed that hindered settling can be interpreted as a limiting case of finite-strain consolidation when effective stress is reduced to zero. Buscall (1990) demonstrated that sedimentation modeled using osmotic pressure gradients and consolidation described through effective stress gradients are mathematically equivalent under appropriate assumptions. Toorman (1996) later derived a unified framework based on two-phase conservation equations, showing that both Kynch sedimentation and Gibson's large-strain consolidation equation emerge as special cases of a single governing advection–diffusion formulation (Chassagne, 2021).

The mathematical challenge lays in the implementation of the transition between the sedimentation and consolidation phases and will be discussed in the present article.

Classical consolidation theory can be viewed as describing the regime where effective stress is dominant. Terzaghi (1925) formulated one-dimensional small-strain consolidation under the assumptions of vertical deformation and vertical drainage. This approach works well for moderate settlements and relatively stiff soils, but it becomes inadequate for very soft materials where settlements are large and material properties evolve significantly during compression. Gibson and MJL (1967), Gibson et al. (1981) addressed this limitation by introducing large-strain consolidation theory, reformulating the governing equations in material coordinates so that changes in layer thickness, void ratio, and permeability are consistently captured. This framework is particularly relevant for materials that originate as suspensions and undergo substantial volumetric changes during consolidation.

The hydraulic description was later extended to include the effect of installed drains. Early work by Barron (1948) and Hansbo (1981) introduced radial drainage toward the drains, while still assuming that the soil deforms only in the vertical direction. More recent studies have combined radial drainage with large-strain behavior and nonlinear material properties, and also included practical effects such as smear (disturbance of the soil around the drain) and well resistance (limited flow capacity inside the drain) (Indraratna et al., 2017; Geng and Yu, 2017). These approaches have also been adapted to horizontal drains (Li et al., 2025), allowing water to flow in multiple directions while keeping the deformation vertical. These models remain effective because, in very soft soils improved with drains, settlement is mainly driven by gravity in the vertical direction, while horizontal deformation stays relatively small under uniform loading and lateral confinement.

From a broader continuum-mechanics perspective, these simplified sedimentation–consolidation models may be contrasted with fully coupled poromechanical formulations. In small-strain Biot theory (Biot, 1941, 1955), consolidation is written as a coupled displacement–pore pressure problem with full tensorial stress representation. Finite-strain poromechanics formulations developed by Borja and co-workers (Borja et al., 1998a; Borja and Alarcón, 1995; Borja et al., 1998b) extend this framework to large deformations and nonlinear constitutive behavior. Although these approaches are more general and can naturally represent multilayered systems, stress redistribution, and plasticity effects, they introduce significant computational complexity and require a larger number of constitutive parameters. In contrast, large-strain sedimentation–consolidation and drain models focus on the dominant gravity-driven mechanisms, namely vertical settlement, evolving geometry, and multidirectional drainage, while avoiding the full tensorial and plastic complexity of fully coupled formulations. For problems governed primarily by vertical settlement under laterally constrained conditions, these approaches provide a physically consistent framework for analyzing very soft soils while retaining a relatively simple constitutive description.

Recent studies have also explored data-driven, physics-informed, and digital-twin approaches for improving consolidation settlement predictions using monitoring data and numerical model updating (Tian and Wang, 2023; Tian et al., 2025). These approaches focus on updating the response of existing soil deposits or geotechnical structures as new observations become available. In contrast, the present work addresses the earlier sediment-to-soil transition and proposes a unified large-strain framework capable of describing the evolution from a dilute suspension to a consolidated soil within a single formulation.

Despite the significant advances achieved in sedimentation theory, large-strain consolidation modeling, drainage-enhanced consolidation, and data-assisted prediction methods, a unified numerical framework capable of describing the complete transition from dilute suspension to self-weight consolidation within a single finite-strain formulation remains relatively uncommon. This limitation is particularly relevant for hydraulically dredged sediments, where sedimentation and consolidation occur as successive stages of the same physical process.

This paper presents a unified finite element framework for describing the full evolution of soft clay suspensions from sedimentation to self-weight consolidation. The formulation is built from a common set of governing equations and constitutive relations that allow both regimes to be represented within a single continuous model. The paper first introduces the theoretical framework, notations, and governing equations, and then derives the unified advection–diffusion formulation used for both sedimentation and consolidation. Numerical aspects such as the smooth transition around the gelling concentration and the stabilization of advection-dominated transport are then discussed. The model is validated against experimental results for suspensions of kaolinite clay in water and a natural mud sampled from the Marker Wadden (The Netherlands) in both one-dimensional and drainage-controlled configurations. Finally, the framework is compared with a more general large-strain finite element formulation based on logarithmic compressibility in order to assess its consistency, range of applicability, and practical relevance for geotechnical engineering problems.

2. Functional setting

The finite-element formulation adopted in this work is based on the classical weak (variational) form of the governing equations (Zienkiewicz et al., 2013; Hughes, 2012). In this approach, the governing equations are not solved directly in their strong form. Instead, they are reformulated into an equivalent weak form, which provides the basis for the finite-element discretization.

Let $\Omega_0 \subset \mathbb{R}^d$ denote the reference domain and $\partial\Omega_0$ its boundary. The solution is sought in the Sobolev space $H^1(\Omega_0)$, which contains functions whose values and first derivatives are square-integrable. This level of regularity is sufficient for the weak formulation considered in this work (Ern and Guermond, 2004).

The boundary is decomposed into Dirichlet and Neumann parts, $\partial\Omega_D$ and $\partial\Omega_N$, respectively. The trial space V contains all admissible solutions satisfying the prescribed Dirichlet boundary conditions, while the test space V_0 contains admissible variations that vanish on the Dirichlet boundary. These spaces are defined as

$$\partial\Omega_0 = \partial\Omega_D \cup \partial\Omega_N, \qquad \partial\Omega_D \cap \partial\Omega_N = \emptyset.$$

We introduce the Sobolev space

$$H^1(\Omega_0) = \left\{ v \in L^2(\Omega_0) \;\middle|\; \mathrm{Grad}_{\mathbf{X}} v \in (L^2(\Omega_0))^d \right\},$$

and define the trial space

$$V = \left\{ v \in H^1(\Omega_0) \mid v = \phi_D \text{ on } \partial\Omega_D \right\}, \tag{1}$$

and the corresponding test space

$$V_0 = \left\{ v \in H^1(\Omega_0) \mid v = 0 \text{ on } \partial\Omega_D \right\}. \tag{2}$$

3. Unified theoretical framework

3.1. Problem definition and assumptions

This study considers the sedimentation and self-weight consolidation of fine-grained, water-saturated sediments placed hydraulically, as commonly encountered in land reclamation and in large dewatering fields. The material is initially deposited as a suspension with high water content and progressively evolves toward a dense, load-bearing deposit. The objective is to describe this full evolution within a single, consistent modeling framework.

The sediment is idealized as a two-phase system composed of solid particles and pore water. Only saturated conditions are considered, and the presence of a gas phase is neglected. Gravity acts in the vertical direction and constitutes the primary driving force governing both sedimentation and consolidation, through the self-weight of the sediment and the associated hydrostatic response of the pore fluid. Thermal, chemical, and biological effects are not included, and the material is assumed to be isothermal and chemically homogeneous over the timescales of interest.

External mechanical loads may be applied, but only in the form of spatially uniform, vertically applied loads, consistent with the large-scale, one-dimensional or plane-strain conditions typical of land reclamation practice. Localized, non-uniform, or shear-dominated loading conditions are therefore outside the scope of the present framework.

The mechanical response spans two connected regimes. At low solid concentrations, particles settle relative to the fluid, and the material behaves as a suspension in which particle motion is controlled by gravity, viscous drag, and colloidal interactions. As the solid concentration increases, interparticle contacts develop and a connected network forms at a critical concentration, referred to as the gelling concentration. Beyond this point, the material behaves as a deformable porous skeleton, and deformation is governed by effective stresses within the solid matrix and dissipation of pore water pressure. Although the underlying physical mechanisms differ across these regimes, both are described here using the same governing balance laws combined with appropriate constitutive relations.

Large deformations are expected during both sedimentation and self-weight consolidation, particularly for soft sediments with high initial water content. The formulation therefore allows for large strains and evolving material properties. Classical small-strain consolidation theory is recovered as a limiting case at later stages, when deformations become small and material properties vary more slowly. In contrast to approaches that switch between different governing equations, the present formulation uses a single continuous framework, in which the transition between sedimentation and consolidation is regularized to provide a continuous description of the problem.

The primary state variable used to describe the material is the solid volume fraction, which provides a continuous measure of density from dilute suspension to dense soil. Pore water pressure and solid deformation are coupled through mass conservation and force equilibrium. Constitutive relations are introduced to link effective stress and permeability to the solid volume fraction, enabling a unified description of both settling-dominated and consolidation-dominated behavior.

The framework is formulated in one dimension for vertical sedimentation and self-weight consolidation and is later extended to two-dimensional configurations to represent drainage effects and homogeneous engineering interventions. Operational aspects such as staged deposition are represented as changes in loading and domain geometry rather than as separate physical processes. These assumptions define the scope of the model and focus the analysis on the dominant gravity-driven mechanisms relevant to land reclamation applications.

3.2. Governing equations

The suspension is modeled as a saturated porous medium composed of a solid phase and a pore fluid. The formulation is expressed in a Lagrangian framework attached to the solid phase, which is well suited for describing the large deformations occurring during sedimentation and self-weight consolidation. Inertia effects are neglected for self-weight consolidation, and gravity is assumed to be the dominant driving force.

Mass balance of the solid phase. The conservation of solid mass is first written in the Eulerian configuration as

$$\frac{\partial \phi_s}{\partial t} + \mathrm{div}_{\mathbf{x}}\left(\phi_s \mathbf{v}_s\right) = 0, \tag{3}$$

where ϕ_s is the solid volume fraction and $\mathbf{v}_s$ is the solid velocity.

Introducing the material derivative following the solid phase,

$$\frac{D}{Dt}(\cdot) = \frac{\partial}{\partial t}(\cdot) + \mathbf{v}_s \cdot \mathrm{grad}_{\mathbf{x}}(\cdot), \tag{4}$$

the solid mass balance becomes

$$\frac{D\phi_s}{Dt} + \phi_s \,\mathrm{div}_{\mathbf{x}}(\mathbf{v}_s) = 0. \tag{5}$$

Mass balance of the fluid phase. The conservation of fluid mass in the Eulerian configuration reads

$$\frac{\partial \phi_w}{\partial t} + \mathrm{div}_{\mathbf{x}}\left(\phi_w \mathbf{v}_w\right) = 0, \tag{6}$$

where $\phi_w = 1 - \phi_s$ is the fluid volume fraction and $\mathbf{v}_w$ is the fluid velocity.

Expressed in terms of the material derivative following the solid phase, the fluid mass balance becomes

$$\frac{D\phi_w}{Dt} + \mathrm{div}_{\mathbf{x}}(\mathbf{J}_{w/s}) + \phi_w \,\mathrm{div}_{\mathbf{x}}(\mathbf{v}_s) = 0, \tag{7}$$

where $\mathbf{J}_{w/s} = \phi_w(\mathbf{v}_w - \mathbf{v}_s)$ is the fluid flux relative to the solid skeleton.

Momentum balance. Under quasi-static conditions relevant for sedimentation and consolidation, the balance of linear momentum for the mixture, expressed in the current configuration, reduces to

$$\mathrm{div}_{\mathbf{x}}(\boldsymbol{\sigma}) + \rho \mathbf{g} = \mathbf{0}, \tag{8}$$

where $\boldsymbol{\sigma}$ is the Cauchy stress tensor, ρ is the bulk density, and $\mathbf{g}$ is the gravitational acceleration.

Coupling and dimensional reduction. The governing equations are coupled through the deformation of the solid skeleton, the pore fluid pressure, and the relative fluid flux. In the applications considered in this study, deformation and flow are predominantly vertical, allowing the governing equations to be reduced to a one-dimensional form. The general Lagrangian formulation nevertheless provides a consistent basis for extension to two-dimensional configurations, as demonstrated later for drainage problems.

To close the system of equations, constitutive relations are required to relate effective stress and permeability to the solid volume fraction. These relations are introduced in the following subsection.

4. Coupling sedimentation and consolidation

4.1. Advection–diffusion formulation

Sedimentation and consolidation are both governed by the mass-balance equations introduced in Section 3.2. The transition between these two regimes does not arise from changes in the governing balance laws themselves, but from changes in the dominant transport mechanisms. In this section, a single transport equation is derived to describe the evolution of the solid volume fraction throughout the entire process, from sedimentation to consolidation.

By combining the solid and fluid mass-balance equations in their Lagrangian form, Eqs. (5) and (7), and by expressing the water volume fraction ϕ_w and the solid velocity relative to the reference frame in terms of the solid volume fraction ϕ_s and its material derivative, the following evolution equation is obtained:

$$\frac{1}{\phi_s}\frac{D\phi_s}{Dt} - \mathrm{div}_{\mathbf{x}}\left(\mathbf{J}_{w/s}\right) = 0, \tag{9}$$

which governs the evolution of the solid volume fraction in both the sedimentation and consolidation regimes.

Expressed in the Lagrangian reference configuration, this equation becomes

$$\frac{1}{\phi_s}\frac{D\phi_s}{Dt} - \frac{1}{J}\mathrm{Div}_{\mathbf{X}}\left(J\,\mathbf{F}^{-1}\mathbf{J}_{w/s}\right) = 0, \tag{10}$$

where $\mathbf{X}$ denotes the Lagrangian coordinate vector, $\mathbf{F}$ is the deformation gradient defined as

$$\mathbf{F} = \mathrm{grad}_{\mathbf{x}}(\mathbf{u}) + \mathbf{I},$$

with $\mathbf{u} = \mathbf{x} - \mathbf{X}$ the displacement field, and $J = \det(\mathbf{F})$ is the Jacobian of the deformation gradient. For incompressible solid particles, the Jacobian is directly related to the solid volume fraction through

$$J = \frac{\phi_0}{\phi_s}, \tag{11}$$

where ϕ_0 is the reference solid volume fraction.

A detailed derivation of Eqs. (9)–(10), including the definition and sign convention of $\mathbf{J}_{w/s}$ and the Eulerian-to-Lagrangian transformation, is provided in Supplementary Material.

The relative water flux $\mathbf{J}_{w/s}$ is decomposed into advective and diffusive contributions,

$$\mathbf{J}_{w/s} = \mathbf{J}^{\mathrm{adv}}_{w/s} + \mathbf{J}^{\mathrm{diff}}_{w/s}, \tag{12}$$

where each term represents a distinct physical transport mechanism. This decomposition is applied in both regimes and allows regime-specific constitutive relations to be introduced without altering the mathematical structure of the governing equation.

The advective flux $\mathbf{J}^{\mathrm{adv}}_{w/s}$ represents transport due to the bulk motion of the suspension relative to the solid skeleton. It is primarily driven by gravity and fluid viscosity and is active in both sedimentation and consolidation. During sedimentation, advection corresponds to particle settling relative to the pore fluid, whereas during consolidation it represents drainage induced by the self-weight of the solid skeleton.

The diffusive flux $\mathbf{J}^{\mathrm{diff}}_{w/s}$ represents transport driven by gradients in the solid volume fraction. Although its mathematical form is identical in both regimes, the underlying physical mechanisms differ. In the sedimentation regime, diffusion is mainly governed by colloidal interactions such as Brownian motion and electrostatic repulsion. In the consolidation regime, diffusion arises from inter-particle contact forces and the deformation of the solid skeleton. These differences are captured through appropriate constitutive expressions for the diffusive flux, which are introduced in the following subsections.

This advection–diffusion formulation therefore provides a single governing equation for the evolution of the solid volume fraction, with sedimentation and consolidation emerging as limiting cases determined by the dominant transport mechanisms and their associated constitutive descriptions.

4.2. Sedimentation regime

4.2.1. Advective flux in the sedimentation regime

A single spherical particle suspended in a viscous fluid settles under the combined action of gravity and viscous drag. Assuming force equilibrium and neglecting inertial effects, the settling velocity is given by the classical Stokes solution. The terminal settling velocity of an isolated spherical particle is expressed as

$$\mathbf{v}_0 = \frac{(\rho_s - \rho_w)\,V_p}{6\pi\eta a}\,\mathbf{g}, \tag{13}$$

where $\mathbf{v}_0$ is the Stokes settling velocity, η is the dynamic viscosity of the fluid, V_p is the particle volume, a is the particle radius, ρ_s is the solid density, ρ_w is the fluid density, and $\mathbf{g}$ is the gravitational acceleration vector.

In a suspension, particles do not settle independently but interact, through hydrodynamic forces, with neighboring particles. These interactions reduce the mobility of individual particles and lead to a decrease in the effective settling velocity, a phenomenon commonly referred to as hindered settling. This effect is typically modeled by multiplying the Stokes settling velocity by a concentration-dependent reduction factor smaller than unity.

The settling velocity of the suspension–clear fluid interface is commonly described using the Richardson–Zaki relation (Richardson and Zaki, 1997),

$$\mathbf{v}^{\mathrm{adv}}_s = \mathbf{v}_0\,f(\phi_s) = \mathbf{v}_0\left(1 - \frac{\phi_s}{\phi_{\mathrm{gel}}}\right)^m, \tag{14}$$

where ϕ_s is the solid volume fraction of the suspension (equal to the initial concentration, $\phi_s = \phi_0$), ϕ_{gel} is the gelling concentration, and m is an empirical exponent. In practice, m is typically larger than 5 for non-spherical particles (Chassagne, 2019).

We define the sedimentation hydraulic conductivity tensor $\mathbf{K}^{\mathrm{sed}}_w$ as

$$\mathbf{K}^{\mathrm{sed}}_w = \frac{\|\mathbf{v}_0\|}{\phi_s\left(\dfrac{\rho_s}{\rho_w} - 1\right)}\,f(\phi_s)\,\mathbf{I}. \tag{15}$$

4.2.2. Diffusive flux in the sedimentation regime

The Carnahan–Starling model (Carnahan and Starling, 1969) provides an analytical description of Brownian diffusion in concentrated particle suspensions by accounting for excluded-volume effects. The model expresses the concentration-dependent osmotic pressure through a compressibility factor given by

$$Z(\phi_s) = \frac{1 + \phi_s + \phi_s^2 - \phi_s^3}{(1-\phi_s)^3}, \tag{16}$$

where ϕ_s denotes the solid volume fraction.

In sedimentation models, this relation is commonly used as a diffusion closure linking Brownian motion to gradients in particle concentration. The Carnahan–Starling model captures the rapid increase in diffusive resistance with increasing solid volume fraction and is therefore well suited for describing the diffusion-dominated sedimentation regime below the gelling concentration.

Expressed in terms of a thermodynamic potential, the osmotic pressure reads

$$\Pi(\phi_s) = \frac{k_B T}{V_p}\,\phi_s\,Z(\phi_s), \tag{17}$$

where k_B is the Boltzmann constant, T is the absolute temperature, and V_p is the particle volume.

4.2.3. Sedimentation equation

The flux of colloidal particles during sedimentation is described following the formulation presented in Chapter 12, p. 394 of Russel et al. (1991) and can be written in the general form

$$\mathbf{J}^{\mathrm{sed}}_s = \phi_s\,\mathbf{v}_0\,f(\phi_s) - D_0\,f(\phi_s)\,\mathrm{grad}_{\mathbf{x}}\left(\phi_s Z(\phi_s)\right), \tag{18}$$

where

$$D_0 = \frac{k_B T}{6\pi\eta a} \tag{19}$$

is the thermodynamic diffusion coefficient.

The first term in Eq. (18) represents the advective contribution associated with particle settling, whereas the second term corresponds to the diffusive contribution driven by gradients in solid volume fraction. Using conservation of mass between the solid and fluid phases, the following relation holds:

$$\phi_s\,\mathbf{J}^{\mathrm{sed}}_{w/s} = -\mathbf{J}^{\mathrm{sed}}_s. \tag{20}$$

4.3. Consolidation regime

4.3.1. Advective flux in the consolidation regime

During consolidation, the downward motion of solid particles under gravity is constrained by the rate at which pore water can be expelled from the soil surface. The resulting flow is primarily governed by the pore geometry of the soil and by gradients of excess pore-water pressure generated during consolidation. The water flow relative to the solid skeleton is described by Darcy's law (Darcy, 1856):

$$\mathbf{J}_{w/s}^{\mathrm{cons}} = -\frac{\mathbf{K}_w^{\mathrm{cons}}}{\rho_w g}\,\mathrm{grad}_{\mathbf{x}}\left(p_w + \rho_w g z\right), \tag{21}$$

where $\mathbf{J}_{w/s}^{\mathrm{cons}}$ denotes the water mass flux relative to the solid skeleton, $\mathbf{K}_w^{\mathrm{cons}}$ is the (possibly anisotropic) hydraulic conductivity tensor, allowing for direction-dependent permeability of the soil, ρ_w is the water density, g is the gravitational acceleration, and $\mathrm{grad}_{\mathbf{x}}$ is the spatial gradient operator, p_w is the pore-water pressure, and z is the elevation coordinate. Flow is therefore driven by gradients of the total hydraulic potential and occurs in the direction of decreasing potential.

For isotropic materials, the hydraulic conductivity tensor reduces to

$$\mathbf{K}_w^{\mathrm{cons}} = K_w^{\mathrm{cons}}(\phi_s)\,\mathbf{I}, \tag{22}$$

where K_w^{cons} is a scalar hydraulic conductivity that depends on the solid volume fraction ϕ_s. Merckelbach et al. (2002) proposed a fractal model linking these quantities,

$$K_w^{\mathrm{cons}}(\phi_s) = K_k\,\phi_s^{-n}, \tag{23}$$

with $n = \frac{2}{3-D_f}$. The empirical parameter K_k controls the hydraulic magnitude, while D_f characterizes the pore connectivity and structure. This relation can be readily extended to anisotropic materials by applying the same principle to the eigenvalues of the tensor $\mathbf{K}_w^{\mathrm{cons}}$.

4.3.2. Diffusive flux in the consolidation regime

During consolidation, inter-particle contact forces represented by the effective stress act as diffusion-driving forces. The relationship between the total stress applied to the solid–fluid mixture and the effective stress carried by the solid skeleton is given by Terzaghi's equation (Terzaghi, 1925):

$$\boldsymbol{\sigma}_{sk} = \boldsymbol{\sigma} + p_w\,\mathbf{I}, \tag{24}$$

where $\boldsymbol{\sigma}_{sk}$ denotes the effective stress tensor carried by the solid skeleton, $\boldsymbol{\sigma}$ is the total Cauchy stress tensor, p_w is the pore-water pressure, and $\mathbf{I}$ is the second-order identity tensor. Only the effective stress $\boldsymbol{\sigma}_{sk}$ governs inter-particle contact forces and consolidation.

In the present sedimentation–consolidation framework, the material is assumed to exhibit negligible resistance to pure shear deformation, and viscous stresses are neglected at the scale of large-field self-weight consolidation. Under these assumptions, the stress tensor is represented by its spherical stress component only. For isotropic materials, the effective stress tensor therefore reduces to

$$\boldsymbol{\sigma}_{sk} = -\sigma_{sk}(\phi_s)\,\mathbf{I}, \tag{25}$$

where σ_{sk} is the scalar effective stress, taken positive in compression, and depends on the solid volume fraction ϕ_s. Merckelbach et al. (2002) proposed a fractal relation for this dependence,

$$\sigma_{sk}(\phi_s) = K_\sigma\,\phi_s^n, \tag{26}$$

where

$$n = \frac{2}{3-D_f}, \tag{27}$$

contains the same fractal dimension D_f as used in the permeability model, and whereby K_σ is an empirical parameter that controls the magnitude of the effective stress.

4.3.3. Consolidation flux

The water flow relative to the solid skeleton during the consolidation phase can be written as follows:

$$\mathbf{J}_{w/s}^{\mathrm{cons}} = \frac{\mathbf{K}_w^{\mathrm{cons}}}{\rho_w g}\,\phi_s(\rho_s - \rho_w)\,\mathbf{g} - \frac{\mathbf{K}_w^{\mathrm{cons}}}{\rho_w g}\,\mathrm{grad}_{\mathbf{x}}(\sigma_{sk}), \tag{28}$$

where the first term represents the advective contribution associated with self-weight loading, and the second term represents the diffusive contribution driven by gradients of effective stress.

4.4. Strong general equation of sedimentation and consolidation

Both sedimentation and consolidation can be expressed within a unified advection–diffusion framework. In the Lagrangian configuration, the governing equation for the solid volume fraction reads

$$C(\phi_s)\,\frac{D\phi_s}{Dt} - \mathrm{Div}_{\mathbf{X}}\left[\mathbf{D}_{\mathrm{diff}}^{\mathrm{eq}}\,\mathrm{Grad}_{\mathbf{X}}\phi_s\right] + \mathbf{V}_{\mathrm{adv}}^{\mathrm{eq}}\cdot\mathrm{Grad}_{\mathbf{X}}\phi_s = 0, \tag{29}$$

where the compressibility term is defined as

$$C(\phi_s) = \frac{J}{\phi_s}, \tag{30}$$

the equivalent diffusion tensor is given by

$$\mathbf{D}_{\mathrm{diff}}^{\mathrm{eq}} = J\,\mathbf{F}^{-1}\,\frac{\mathbf{K}_w^{\mathrm{eq}}}{\rho_w g}\,\mathbf{F}^{-T}\,\Gamma^{\mathrm{eq}}, \tag{31}$$

and the equivalent advective velocity reads

$$\mathbf{V}_{\mathrm{adv}}^{\mathrm{eq}} = \frac{\partial \mathbf{W}_{\mathrm{adv}}^{\mathrm{eq}}}{\partial \phi_s} = \frac{\partial}{\partial \phi_s}\left[J\,\mathbf{F}^{-1}\,\frac{\mathbf{K}_w^{\mathrm{eq}}}{\rho_w g}\,\phi_s(\rho_s-\rho_w)\,\mathbf{g}\right]. \tag{32}$$

Here, $\mathbf{K}_w^{\mathrm{eq}}$ denotes an equivalent hydraulic conductivity tensor, and Γ^{eq} represents an equivalent driving potential gradient, defined as

$$\mathbf{K}_w^{\mathrm{eq}}(\phi_s) = \begin{cases} \mathbf{K}_w^{\mathrm{sed}}(\phi_s), & \phi_s < \phi_{\mathrm{gel}}, \\ \mathbf{K}_w^{\mathrm{cons}}(\phi_s), & \phi_s \geq \phi_{\mathrm{gel}}, \end{cases} \tag{33}$$

$$\Gamma^{\mathrm{eq}}(\phi_s) = \begin{cases} \dfrac{1}{\phi_s}\,\dfrac{D_0}{\|\mathbf{v}_0\|}\,\dfrac{\partial\left[\phi_s Z(\phi_s)\right]}{\partial \phi_s}, & \phi_s < \phi_{\mathrm{gel}}, \\ \dfrac{\partial \sigma_{sk}}{\partial \phi_s}(\phi_s), & \phi_s \geq \phi_{\mathrm{gel}}. \end{cases} \tag{34}$$

The function $C(\phi_s)$ characterizes the compressibility of the material, $\mathbf{V}_{\mathrm{adv}}^{\mathrm{eq}}$ represents the Lagrangian advective velocity associated with variations in solid volume fraction, and $\mathbf{D}_{\mathrm{diff}}^{\mathrm{eq}}$ is the corresponding diffusion tensor governing the transport of the solid phase.

Weak formulation. The weak form is obtained by multiplying Eq. (29) by a test function $\psi \in V_0$, integrating over Ω_0, and applying integration by parts to the diffusive term.

The variational problem reads:

Find $\phi_s \in V$ such that

$$\int_{\Omega_0} C(\phi_s)\,\frac{D\phi_s}{Dt}\,\psi\,\mathrm{d}\Omega + \int_{\Omega_0} \mathbf{D}_{\mathrm{diff}}^{\mathrm{eq}}\,\mathrm{Grad}_{\mathbf{X}}\phi_s\cdot\mathrm{Grad}_{\mathbf{X}}\psi\,\mathrm{d}\Omega - \int_{\Omega_0} \mathbf{W}_{\mathrm{adv}}^{\mathrm{eq}}\cdot\mathrm{Grad}_{\mathbf{X}}\psi\,\phi_s\,\mathrm{d}\Omega = \int_{\partial\Omega_N} J\,\mathbf{F}^{-1}\mathbf{q}_w\cdot\mathbf{N}\,\psi\,\mathrm{d}\Gamma, \tag{35}$$

for all $\psi \in V_0$.

Here, $\mathbf{q}_w$ denotes the prescribed water flux defined in the current configuration, while the term $J\,\mathbf{F}^{-1}\mathbf{q}_w$ represents its pull-back to the reference configuration Ω_0.

5. Numerical treatment

5.1. Discontinuity

The discontinuous nature of the sedimentation–consolidation transition poses significant challenges for numerical modeling. To address

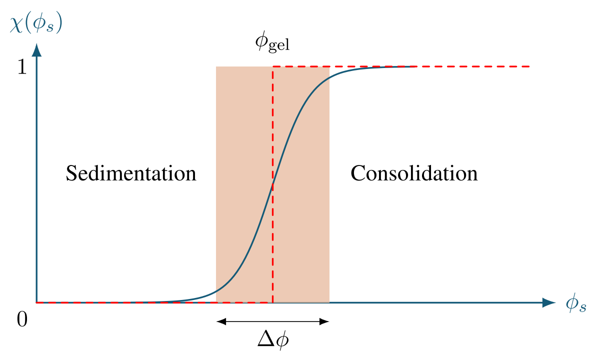

Fig. 1. From a discontinuous transition at ϕ_{gel} to a smooth transition over the interval $[\phi_{gel} - \Delta\phi, \phi_{gel} + \Delta\phi]$. The transition is described by the function $\chi(\phi_s)$.

this difficulty, a transition regime is introduced in which a smooth and continuous interpolation between sedimentation and consolidation is enforced, ensuring numerical stability and physical consistency.

The transition between Eqs. (18) and (28) is introduced through a smooth interpolation function defined as

$$\mathbf{K}_w^{eq}(\phi_s) = \mathbf{K}_w^{sed}(\phi_s)\,\left(1 - \chi(\phi_s)\right) + \mathbf{K}_w^{cons}(\phi_s)\,\chi(\phi_s), \tag{36}$$

which ensures a continuous transition between the sedimentation and consolidation regimes.

Brownian motion is always present, including after the onset of consolidation, and is therefore continuously accounted for in the formulation. The transition function is applied only to the contact-force contribution, which becomes significant once consolidation begins. The resulting expression for the effective driving potential reads

$$\Gamma^{eq}(\phi_s) = \frac{1}{\phi_s}\frac{D_0}{\|\mathbf{v}_0\|}\frac{\partial\left[\phi_s Z(\phi_s)\right]}{\partial\phi_s} + \frac{\partial\sigma_{sk}(\phi_s)}{\partial\phi_s}\,\chi(\phi_s), \tag{37}$$

The transition function $\chi(\phi_s)$ is chosen as a logistic (sigmoid) function that varies smoothly from 0 to 1 around the gelling concentration ϕ_{gel} (see Fig. 1). It is defined as

$$\chi(\phi_s) = \frac{1}{1 + \exp\left[-\alpha\left(\phi_s - \phi_{gel}\right)\right]}, \tag{38}$$

where ϕ_s is the solid volume fraction, ϕ_{gel} is the gelling concentration, and α is a dimensionless parameter controlling the sharpness of the transition. For the chosen value $\alpha = 2000$, the transition remains very sharp while avoiding discontinuities. More generally, the width of the transition can be estimated by considering the interval over which the function χ varies between two values ε and $1-\varepsilon$. From Eq. (38), this interval is given by

$$\Delta\phi_= \frac{2}{\alpha}\ln\left(\frac{1-\varepsilon}{\varepsilon}\right).$$

For instance, taking $\varepsilon = 0.05$ (i.e. $\chi \in [0.05, 0.95]$) yields

$$\Delta\phi = \frac{\ln(19)}{\alpha} \approx 3\times10^{-3}.$$

This shows that the transition is confined to a very narrow range around ϕ_{gel}, ensuring a behavior that is close to discontinuous while remaining numerically stable.

5.2. SUPG for advection-dominant regime

In the sedimentation regime, transport is often strongly advection-dominated, as particle settling under gravity prevails over diffusive effects. Under these conditions, the governing equation becomes convection-dominated and standard numerical discretizations may produce non-physical oscillations, particularly at high Péclet numbers. These oscillations occur because central discretization schemes do not provide sufficient numerical damping to stabilize sharp concentration fronts transported by the flow. In classical finite-difference methods, this issue is typically addressed using upwinding, where spatial derivatives are evaluated according to the direction of the flow. This approach introduces a small amount of artificial diffusion aligned with the advective direction, which suppresses spurious oscillations while preserving the correct transport behavior. The same stabilization principle was later extended to the finite element framework through methods such as streamline upwind and Petrov–Galerkin formulations, which introduce directional stabilization along streamlines to ensure stable and physically consistent solutions in advection-dominated regimes. This method was first derived by Brooks and Hughes (1982) and later improved by numerous authors.

Starting from the weak formulation given in Eq. (35), stabilization is introduced through a modified test function in the spirit of the Streamline Upwind/Petrov–Galerkin (SUPG) method proposed by Brooks and Hughes (1982). Instead of using the standard Galerkin test function $\psi_h \in V_h$, a stabilized test function is defined as

$$\psi_h^{SUPG} = \psi_h + \tau_K\,\mathbf{V}_{adv}^{eq}\cdot \mathrm{Grad}_{\mathbf{X}}\psi_h, \tag{39}$$

where τ_K is an element-wise stabilization parameter and $\mathbf{V}_{adv}^{eq}$ denotes the equivalent advective velocity.

In the advection-dominated regime, where diffusive effects are negligible and the element Péclet number is large, the stabilization parameter is commonly approximated as

$$\tau_K \approx \frac{h_K}{2\,\|\mathbf{V}_{adv}^{eq}\|}, \tag{40}$$

where h_K is a characteristic element length. This choice corresponds to classical first-order upwinding and introduces controlled numerical diffusion aligned with the streamline direction. As a result, spurious oscillations are suppressed while maintaining consistency with the original governing equation.

5.3. Numerical implementation considerations

The numerical implementation was designed to preserve the physical advection–diffusion character of the governing equation while maintaining robustness in strongly advection-dominated regimes.

The spatial and temporal discretizations adopted for the different numerical examples are summarized in Table 1. For both the one-dimensional and drainage simulations, the governing equations were solved using a two-dimensional finite-element discretization. For the one-dimensional sedimentation and consolidation cases, a single element was used in the horizontal direction ($n_x = 1$), while the domain width was selected as

$$W = \frac{H}{n_y},$$

where H is the column height and n_y is the number of elements in the vertical direction. This choice ensures that the horizontal and vertical element dimensions remain approximately equal ($\Delta x \approx \Delta y$), resulting in a mesh aspect ratio close to unity. Maintaining nearly square elements was found to be important for the SUPG stabilization, whose stabilization parameter depends on the characteristic element length. Preliminary numerical experiments showed that highly elongated elements may introduce additional numerical diffusion through the stabilization term and affect the sharpness of concentration fronts.

The stabilization term was evaluated explicitly using values from the previous time step. This strategy was adopted because the equivalent advective velocity depends nonlinearly on the solid volume fraction and its derivatives. Including the full SUPG contribution implicitly in the Newton iterations was found to significantly increase the nonlinearity of the resulting system. The explicit treatment therefore improves robustness while preserving the consistency of the formulation.

Table 1
Spatial and temporal discretization adopted for the numerical examples.

Case	Domain size (m)	Mesh	Δx (m)	Δy (m)	Δt (s)
K1 settling columns	0.002×0.20	1 × 100	0.002	0.002	100
Marker Wadden settling columns	0.0045×0.45	1 × 100	0.0045	0.0045	100
Marker Wadden with PVD	0.05×1.20	5 × 100	1.0×10^{-2}	1.2×10^{-2}	1000
PHD benchmark	0.50×0.60	60 × 60	8.33×10^{-2}	1.0×10^{-1}	1000

Because the stabilization contribution is treated explicitly, relatively small time increments were employed during sedimentation-dominated regimes. As shown in Table 1, a typical time step of 100 s was used for the one-dimensional sedimentation problems, which was sufficient to accurately resolve the evolution of the settling front. Once the solution entered the consolidation regime, larger time steps could be employed because the remaining terms of the governing equation are treated implicitly and the solution evolves more smoothly in time. For the drainage simulations, time increments of the order of 1000 s were adopted, providing a good compromise between computational efficiency and numerical accuracy.

6. Material and methods

To evaluate the predictive capability of the proposed sedimentation–consolidation model, simulations were performed for two distinct materials: a well-characterized kaolinite (defined as “K1”) reported in a previous study (Myouri et al., 2025) and a natural mud used in land reclamation project, also reported in a another study (Rial, 2019; Barciela-Rial et al., 2024a). The mud was tested in both a undrained settling column and a column with vertical drainage. The kaolinite K1 serves as a controlled and reproducible reference material. In contrast, the natural mud represents a heterogeneous, field-representative sediment that captures the complexity typically encountered in engineering applications. The combined use of these materials enables a comprehensive assessment of model performance across both idealized laboratory conditions and realistic, practice-oriented scenarios.

Kaolinite K1. The first material consists of kaolinite K1, a commercial kaolinite (Speswhite DAT002K, IMERYS). Kaolinite K1 is composed of micrometer-sized, plate-like aluminosilicate particles with negatively charged basal surfaces and pH-dependent edge charges. Laser diffraction measurements show a bimodal particle-size distribution, with a median particle size D_{50} of approximately 12.5 μm. Suspensions were prepared in deionized water over a wide range of initial concentrations, from 39 to 450 g/L. The density evolution in time was recorded using NMR scanning device (Hol et al., 2025b,a; Myouri et al., 2025) in small tubes of 200 mm high, 23 mm wide cylindrical glass containing roughly 80 mL for each suspension and was used to find the Merkelbach model (see Table 2). The variability of the Merckelbach–Kranenburg parameters are due to the chemical-properties variation in large concentration due to leaching as mentioned in the previous study (Myouri et al., 2025).

Marker Wadden Mud. The second material consists of a natural dredged mud originating from Lake Markermeer in the Netherlands, which was reused in the present drainage and consolidation study. This sediment is the same material used in the Marker Wadden land reclamation project. It corresponds to the fine fraction of the upper lake bed, contains no sand, about 4.5% total organic matter, and has a particle density of approximately 2540 kg/m^3. The gelling concentration of this mud is reported in the range of 70–85 g/L in previous studies.

First, settling experiments were performed in 2-liter columns (height 45 cm, inner diameter 8 cm) for initial concentrations ranging from 40 to 400 g/L. These tests were used to determine the consolidation parameters of the material (see Table 2).

Subsequently, the same mud was reused in a partial vertical drainage setup to investigate its consolidation behavior under controlled hydraulic boundary conditions. For this purpose, a suspension with an initial concentration of 423 g/L was prepared and placed in a vertical cylindrical Perspex column (inner diameter 10 cm, height 120 cm). After filling and remixing, the sediment was allowed to settle and self-weight consolidate for 14 days. This initial period ensured that a stable sediment layer was formed before applying controlled drainage conditions. The start of the drainage experiment was defined after this 14-day pre-consolidation phase.

The column was equipped with a centrally positioned stainless-steel drainage pipe (outer diameter 2 cm) running along its full height. The pipe was perforated over a defined drainage length and covered with porous filters to allow radial inflow of pore water while preventing sediment intrusion. The pipe was connected at its base to an external constant-head reservoir, which imposed a fixed water level inside the column. The volume of drained (or supplied) water was continuously monitored.

This cylindrical, axisymmetric configuration enables controlled radial drainage toward the central pipe and allows assessment of drainage-induced consolidation under well-defined and reproducible boundary conditions. Throughout the experiment, the mud remained fully saturated, as the water level was always maintained above the sediment surface (see Fig. 3).

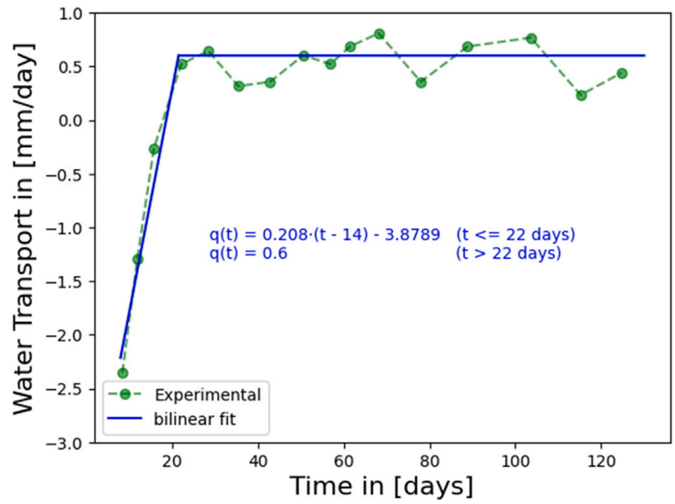

Fig. 2. The elementary water flux from the drainage surface as measured experimentally once the column is connected to the Mariotte bottle after 14 days. The experimental data can be fitted using a bilinear function.

Table 2
The numerical calibration parameters for the modified Gibson used to model the consolidation for different concentration suspensions for kaolinite K1 and Mud.

Type	Concentration in g/L	D_f	K_σ	K_k
K1	450	2.65	3.5e+06	3.8e−12
K1	350	2.65	3.5e+06	3.8e−12
K1	185	2.65	9.0e+06	3e−12
K1	92	2.65	9.0e+06	3e−12
K1	39	2.65	9.0e+06	3e−12
Mud	40–400	2.65	6.5e+06	2e−12

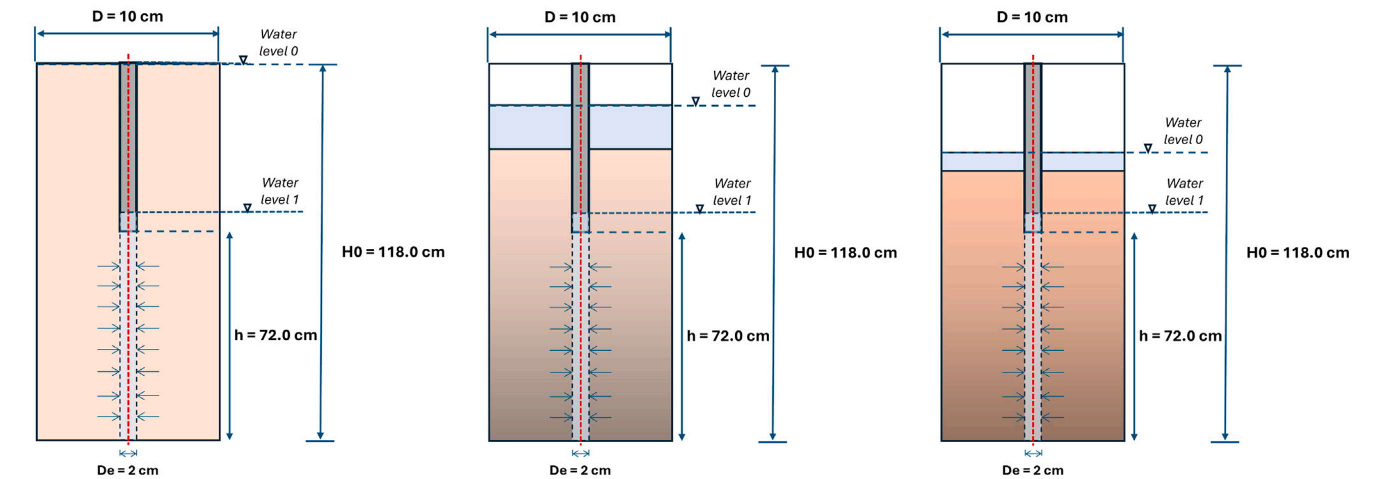

(a) $t = 0$ (initial condition) (b) Intermediate drainage stage (c) Advanced consolidation stage

Fig. 3. Schematic representation of the partial vertical drainage setup at different stages of consolidation. The cylindrical column is equipped with a central drainage pipe connected to a constant-head reservoir, inducing radial flow toward the axis. The material remains fully saturated throughout the experiment, and consolidation occurs under controlled hydraulic boundary conditions.

7. 1D sedimentation–consolidation model results

7.1. Assumptions and boundary conditions

Vertical-deformation dominance. For gravity-driven sedimentation and self-weight consolidation in large-scale fields, lateral deformations and shearing can be neglected, such that $u_x \approx 0$ and $\partial u_y/\partial X \approx 0$. Under this assumption, the deformation gradient can be written directly in terms of the solid volume fraction as

$$\mathbf{F} = \begin{pmatrix} 1 & 0 & 0 \\ 0 & \dfrac{\phi_0}{\phi_s} & 0 \\ 0 & 0 & 1 \end{pmatrix}. \tag{41}$$

Boundary conditions (no drainage, top Dirichlet). To represent a column without drainage, all boundaries are assumed impermeable, except the top boundary where a Dirichlet condition is prescribed on the solid volume fraction. Let Γ_{top} denote the top surface and $\Gamma_{\text{imp}} = \partial\Omega_0 \setminus \Gamma_{\text{top}}$ the remaining boundaries (bottom and side walls). We impose

$$\phi_s = \phi_D(t) \qquad \text{on } \Gamma_{\text{top}}, \tag{42}$$

$$\mathbf{q}_w \cdot \mathbf{n} = 0 \qquad \text{on } \Gamma_{\text{imp}}, \tag{43}$$

where $\mathbf{q}_w$ is the water flux in the current configuration and $\mathbf{n}$ is the outward unit normal. Condition (43) enforces "no drainage" by preventing any net water outflow through the lateral and bottom boundaries. The only exchange is therefore prescribed through the top boundary via (42).

7.2. Kaolinite K1 sedimentation–consolidation

The results for kaolinite K1 show that both the interface evolution and the time-dependent density profiles strongly depend on the initial concentration and on the dominant physical regime.

For intermediate and high concentrations (185, 350, and 450 g/L), the suspension is already in a consolidation-dominated state at deposition (see Figs. 4 and 5). The particles are in contact from the beginning, and self-weight consolidation governs the behavior. In these cases, the interface evolution and the vertical solid volume fraction profiles are well reproduced using only the consolidation parameters derived from the Merckelbach constitutive relations. This confirms that consolidation alone controls the dynamics at high concentrations.

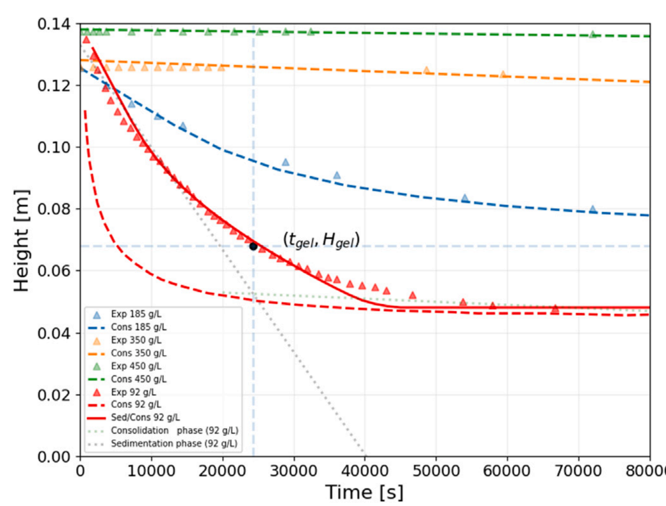

Fig. 4. Interface height evolution for the 92 g/L kaolinite K1 suspension measured by camera monitoring. Comparison between the consolidation-only model and the coupled sedimentation–consolidation model. The identified gel point $(t_{\text{gel}}, H_{\text{gel}})$ marks the transition from sedimentation to consolidation.

In contrast, for the lowest concentration (92 g/L), a clear sedimentation phase occurs before consolidation starts. During this stage, particles settle relative to the fluid, and the interface height decreases approximately linearly with time. Because the consolidation-only model (Cons model) includes only consolidation parameters, it underestimates the interface height and does not reproduce the internal redistribution of solids. This is expected, since it does not account for settling, hindered settling, or flocculation effects.

The sedimentation behavior at low concentration was therefore analyzed separately using direct interface measurements from camera observations, supported by NMR measurements. From the linear part of the interface–time curve, a hindered settling velocity of approximately 4 μ m/s was obtained. The transition from sedimentation to consolidation was identified by a clear change in slope, corresponding to a gelling time of approximately 5 h. Using mass conservation, the corresponding gelling concentration was estimated as

$$\phi_{\mathrm{gel}} \approx 0.072 \quad (\approx 190\ \mathrm{g/L}), \tag{44}$$

and the settling regime was interpreted using a Richardson–Zaki type formulation with an empirical exponent $m \approx 7.4$, consistent with the plate-like shape of kaolinite particles.

In this context, the continuous sedimentation–consolidation model provides a significantly improved description of both the interface evolution and the density profiles at low concentration (see Figs. 4 and 5), particularly near and after the transition from settling to consolidation. This improvement arises from the smooth coupling between sedimentation and consolidation mechanisms, ensuring consistency between interface motion and internal density evolution. The sedimentation–consolidation model captures the curvature of the interface trajectory near the transition and reproduces the gradual development of the density profile over time. In contrast, the consolidation-only model converges to the correct behavior only at late times, when consolidation fully dominates.

Overall, these results demonstrate that a continuous sedimentation–consolidation formulation is necessary to accurately model low-concentration suspensions, while a consolidation-only approach remains appropriate once the material has fully entered the self-weight consolidation regime.

7.3. Marker Wadden mud sedimentation–consolidation

For the Marker Wadden mud, the time evolution of the sediment–water interface also exhibits a clear transition between a settling-dominated regime and a consolidation-dominated regime (see Fig. 7). For the lowest initial concentration (40 g/L), the early-time interface motion is controlled by hindered settling, as reflected by the pronounced change in slope occurring around 10^3–10^4 s. This behavior indicates that, at low concentration, particles are initially not interconnected and settle relative to the pore fluid before a load-bearing network is formed.

In this settling regime, the interface evolution can be described using a Richardson–Zaki type approach, calibrated using a Stokes settling velocity of $v_{\mathrm{Stokes}} = 1.5$ mm/s, consistent with the characteristic particle size of the material. From the fit of the early-time data, a gelling concentration of $\phi_{\mathrm{gel}} \approx 0.075$ (corresponding to approximately 195 g/L) was obtained. Based on the equation (Eq. (14)) and the slope of the suspension of 100 g/L, the parameter m is estimated to be equal to 6.65.

This value is consistent with the observation that suspensions at 200 g/L and above behave predominantly in a consolidation-dominated regime from deposition.

For higher concentrations (200, 300, and 400 g/L), the experimental data show no distinct sedimentation stage (see Fig. 7). Instead, the interface evolution is governed by self-weight consolidation from the beginning of the test. Using the same consolidation parameters across all concentrations, namely $D_f = 2.65$, $K_\sigma = 6.5 \times 10^6$ Pa, and $K_k = 2.0{\times}10^{-12}$ m/s, the numerical solution of the full Gibson equation reproduces the measured interface curves in very good agreement (see Figs. 6 and 7). This confirms that, once the particle network is established, the dynamics are controlled by effective stress development and pore-water drainage.

For concentrations below the gelling threshold, a slight mismatch between data and predictions is observed in the transition range. In particular, for the 100g/L and the 40g/L sample, the model slightly underestimates the early-time interface motion if only consolidation parameters are used. This discrepancy reflects the limitations of a consolidation-only description in the suspension-to-gel transition regime . A far better estimation is observed when incorporating the colloidal behavior into the consolidation model for concentrations below gelling concentrations. The model matches the law of Richardson and Zaki at the sedimentation phase before switching the consolidation phase after the gelling concentration.

In addition to the interface evolution, the density profiles help to better understand the transition between sedimentation and consolidation. Figs. 8 and 9 show the evolution of the solid volume fraction for the 40 g/L and 100 g/L suspensions at different times.

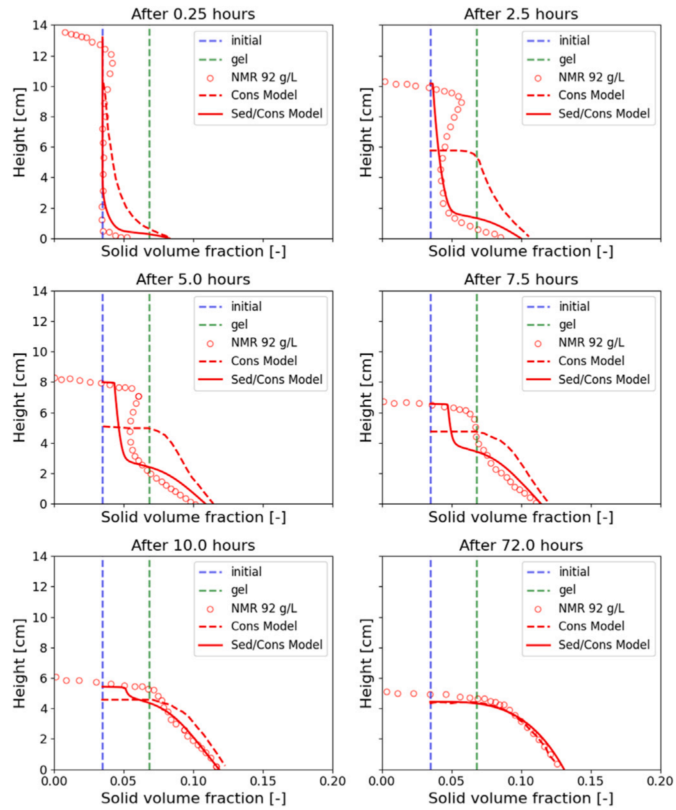

Fig. 5. Comparison between the consolidation-only model and the coupled sedimentation–consolidation model for the 92 g/L kaolinite K1 suspension. Evolution of the solid volume fraction profiles in time as measured by NMR, together with predictions from the consolidation Model and the sedimentation–consolidation Model.

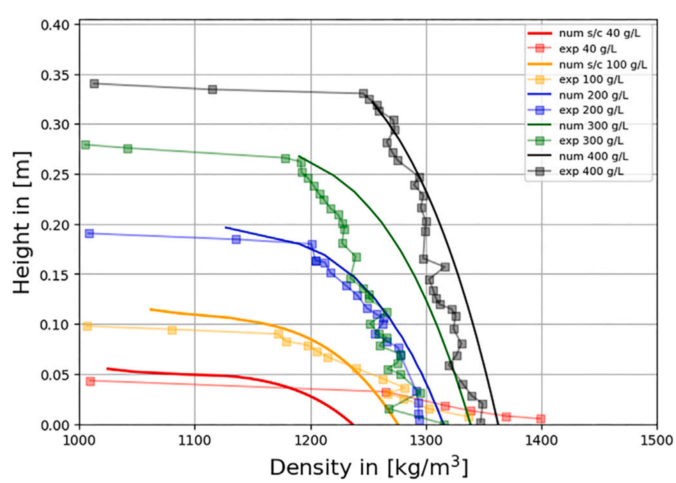

Fig. 6. The final density profile of the Marker Wadden Mud based on density measurements using Ultrasonic High Concentration Meter (UHCM) and the 1d sedimentation–consolidation model for different concentration suspensions.

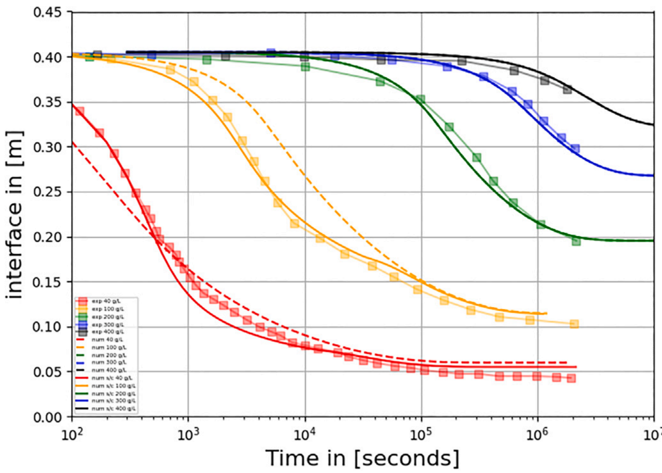

Fig. 7. Evolution of the interface height for Marker Wadden mud at different initial concentrations. Comparison between the 1D consolidation model (solid line) and the coupled 1D sedimentation–consolidation model (dashed line).

At early times, the solid volume fraction remains below the gelling concentration ϕ_{gel}. In this range, particles are not connected and settle independently. As a result, the consolidation-only model predicts almost no change in the profile, while the sedimentation–consolidation model captures the accumulation of solids at the bottom due to settling. As time increases, the profiles progressively reach the gelling concentration. This marks the formation of a connected particle network. After this point, the behavior is dominated by consolidation. Both models then give very similar results. At long times, the profiles almost coincide, showing that the evolution is controlled by effective stress and pore water drainage.

These results explain why the consolidation-only model underestimates the early-time behavior at low concentrations. It cannot capture the initial settling phase. The sedimentation–consolidation model correctly describes both regimes and the transition between them.

7.4. Applicability to other fine-grained sediments

Although the validation presented in this work is limited to kaolinite K1 and Marker Wadden mud, these materials were intentionally selected to represent two contrasting classes of fine-grained sediments. Kaolinite K1 is a relatively clean and well-controlled clay, whereas Marker Wadden mud is a natural sediment characterized by a broader particle-size distribution, organic matter content, and greater material variability.

The objective was therefore to assess the proposed framework under both idealized laboratory conditions and more realistic field conditions. Because the governing equations are formulated independently of a particular material, the framework is not restricted to these two sediments. In principle, other fine-grained clays, silts, and clay–silt mixtures can be considered provided that suitable constitutive relationships and hydraulic properties are available.

Nevertheless, additional validation would be beneficial for materials exhibiting strong structural effects, significant physico-chemical interactions, high organic content, or pronounced anisotropy.

8. Modeling of vertical and horizontal drainage

8.1. Assumptions and boundary conditions

Vertical-deformation dominance. In the presence of vertical drains, pore water flow becomes inherently multi-dimensional, as pressure gradients develop both vertically and radially toward the drain axis. However, for gravity-driven self-weight consolidation of laterally confined soft sediments, shear deformation and lateral strains remain negligible compared to vertical compression. The present formulation therefore assumes one-dimensional vertical deformation of the solid skeleton, while retaining a two-dimensional description of pore water flow. This kinematic constraint reduces mechanical complexity without restricting the hydraulic problem, enabling consistent modeling of radial drainage under large-strain conditions. Thus the deformation tensor is directly linked to the solid volume fraction (Eq. (41)).

Boundary conditions (drainage case). To represent a drained configuration, selected parts of the boundary are allowed to exchange pore water with the exterior, while the remaining boundaries may remain impermeable. Let $\Gamma_{\text{drain}} \subset \partial\Omega_0$ denote the drainage boundary and $\Gamma_{\text{imp}} = \partial\Omega_0 \setminus \Gamma_{\text{drain}}$ the impermeable part of the boundary (e.g., lateral confinement or base).

Drainage may be imposed in two equivalent ways. First, a prescribed water flux (Neumann condition) can be applied,

$$\mathbf{q}_w \cdot \mathbf{n} = q_N(t) \qquad \text{on } \Gamma_{\text{drain}}, \tag{45}$$

$$\mathbf{q}_w \cdot \mathbf{n} = 0 \qquad \text{on } \Gamma_{\text{imp}}, \tag{46}$$

where $\mathbf{q}_w$ is the pore water flux in the current configuration and $\mathbf{n}$ is the outward unit normal.

Alternatively, drainage can be imposed through a prescribed excess pore water pressure (Dirichlet condition),

$$p_e = p_D(t) \quad \text{on } \Gamma_{\text{drain}}, \tag{47}$$

where $p_e = p_w - p_{\text{hyd}}$ denotes the excess pore pressure relative to hydrostatic conditions. In this case, a Dirichlet condition is applied by finding the equivalent solid volume fraction ϕ_{drain} corresponding to the imposed excess pore pressure p_e by solving Terzaghi's equation (Eq. (24)).

Both formulations are consistent with the governing equations. Prescribing $\mathbf{q}_w$ enforces a controlled drainage rate, while prescribing p_e enforces a controlled hydraulic head, allowing the drainage rate to develop naturally from the internal pressure field.

8.2. Partial vertical drainage of Marker Wadden mud

The radial form of the weak equation (see Eq. (35)) was used to account for the cylindrical symmetry of the partial vertical drainage experiments performed on the Marker Wadden mud. This formulation allows radial flow toward the central drainage pipe while maintaining vertical deformation of the solid skeleton. The numerical configuration is illustrated in Fig. 10. The red vertical line represents the prefabricated vertical drain (PVD), along which radial drainage toward the pipe is enforced.

Before the controlled drainage phase begins, the suspension is left in contact with the empty drainage pipe for 14 days. During this period, free drainage occurs and the mud undergoes accelerated consolidation, governed by the imposed water level inside the column. To avoid modeling the detailed hydraulic interaction during this initial phase, the problem was simplified as follows. First, a homogeneous suspension with an initial concentration of 423 g/L was modeled in a 1.18 m high column. The simulation was continued until the sediment height reached the level at which drainage was applied in the experiment, approximately 92.58 cm.

The numerical results show that, under purely self-weight consolidation without forced drainage, approximately 200 days are required to reach this same height. In contrast, the experimental system reaches this state after only 14 days due to free drainage through the pipe.

During the forced drainage phase, Neumann boundary conditions were applied based on the measured water transport values (see Fig. 2). This approach avoids introducing additional assumptions regarding possible clogging of the drainage pipe or the time evolution of the water table.

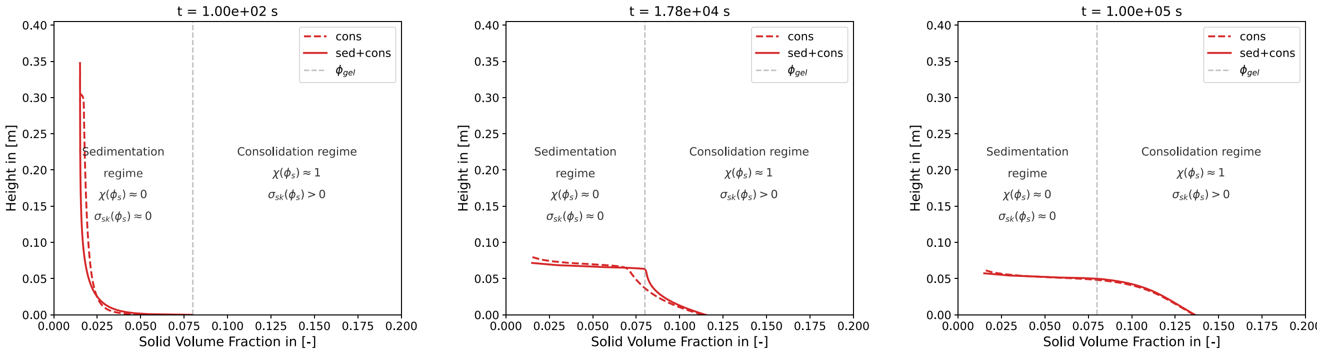

(a) $t = 1.00 \times 10^2$ s (b) $t = 1.78 \times 10^4$ s (c) $t = 1.00 \times 10^5$ s

Fig. 8. Evolution of the solid volume fraction profiles for the 40 g/L suspension at different times. The dashed line corresponds to the consolidation-only model, while the solid line corresponds to the sedimentation–consolidation model. The vertical dashed line indicates the gelling concentration ϕ_{gel}.

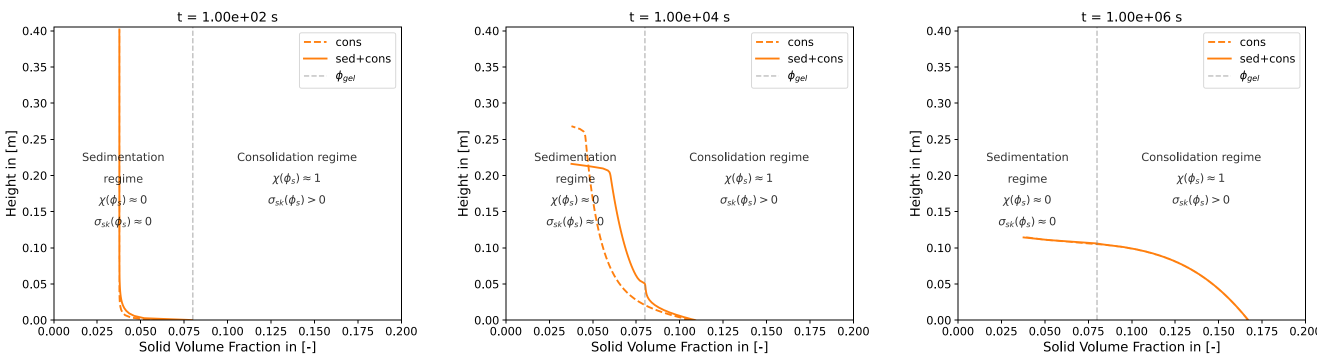

(a) $t = 1.00 \times 10^2$ s (b) $t = 1.00 \times 10^4$ s (c) $t = 1.00 \times 10^6$ s

Fig. 9. Evolution of the solid volume fraction profiles for the 100 g/L suspension at different times. The dashed line corresponds to the consolidation-only model, while the solid line corresponds to the sedimentation–consolidation model. The vertical dashed line indicates the gelling concentration ϕ_{gel}.

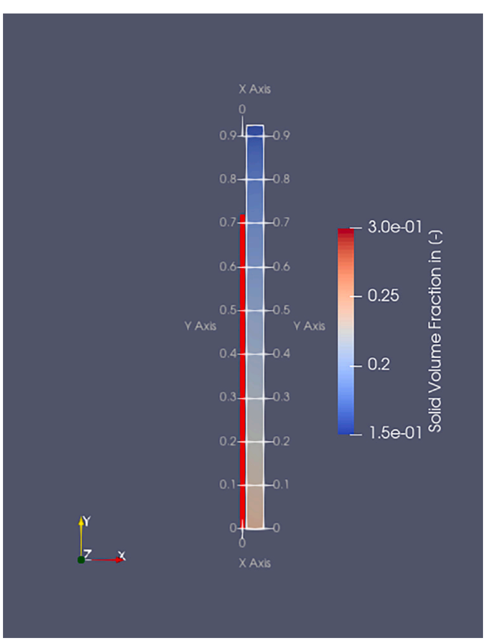

Fig. 10. Axisymmetric representation of the Marker Wadden mud column. The color map shows the solid volume fraction, while the red vertical line represents the prefabricated vertical drain (PVD), acting as a drainage boundary.

Since the initial concentration of 423 g/L is significantly higher than the gelling concentration of the Marker Wadden mud (approximately 195 g/L), the material behaves directly in the consolidation regime. Therefore, only the consolidation parameters were used in the simulations.

The results show good agreement between the model predictions and the experimental measurements in terms of settlement evolution (see Fig. 11).

9. Comparison with full large strain elasto-plastic model

Link between the Merkelbach law and the logarithmic compressibility law. The Merkelbach compressive-strength relation adopted in the consolidation regime is expressed as

$$\sigma_{sk} = K_\sigma \left(\phi_s^n - \phi_0^n\right), \tag{48}$$

where ϕ_s is the solid volume fraction, ϕ_0 is the reference solid fraction, and n is the compressibility exponent.

Using the kinematic relation for incompressible grains (Eq. (11)), the stress expression can be rewritten as

$$\sigma_{sk} = K_\sigma \phi_0^n \left(J^{-n} - 1\right). \tag{49}$$

Introducing the reference stress

$$\sigma_{\text{ref}} = K_\sigma \phi_0^n, \tag{50}$$

leads to

$$J^{-n} = 1 + \frac{\sigma_{sk}}{\sigma_{\text{ref}}}. \tag{51}$$

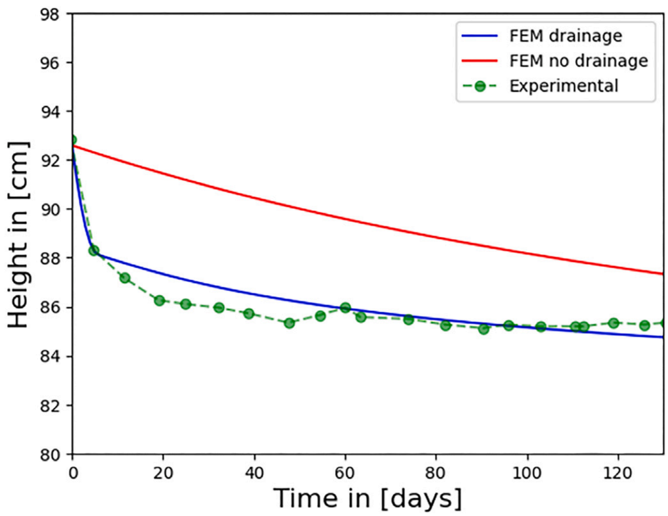

Fig. 11. Comparison between the settlement experimental measurements and the FEM model with and without drainage.

Taking the natural logarithm gives

$$-n \ln J = \ln\left(1 + \frac{\sigma_{sk}}{\sigma_{\mathrm{ref}}}\right). \tag{52}$$

By definition, the volumetric strain is

$$\varepsilon_v = -\ln J, \tag{53}$$

so that

$$\varepsilon_v = \frac{1}{n} \ln\left(1 + \frac{\sigma_{sk}}{\sigma_{\mathrm{ref}}}\right). \tag{54}$$

In the small-strain limit ($J \approx 1$), the volumetric strain can be approximated as

$$\varepsilon_v \approx J - 1. \tag{55}$$

Using the classical relation between the Jacobian and the void ratio,

$$J = \frac{1+e}{1+e_0}, \tag{56}$$

it follows that

$$\varepsilon_v = -\frac{\Delta e}{1+e_0}. \tag{57}$$

Substituting into Eq. (54) yields

$$\frac{\Delta e}{1+e_0} = -\frac{1}{n} \ln\left(1 + \frac{\sigma_{sk}}{\sigma_{\mathrm{ref}}}\right). \tag{58}$$

Eq. (58) has the same logarithmic structure as the classical void ratio–effective stress relationship,

$$e = e_0 - C_0 \ln\left(\frac{\sigma_{sk} + \sigma_{\mathrm{ref}}}{\sigma_{\mathrm{ref}}}\right), \tag{59}$$

with the identification

$$C_0 = \frac{1+e_0}{n}. \tag{60}$$

This demonstrates that, in the small-strain limit, the Merkelbach power-law compressibility is mathematically equivalent to a standard single-slope logarithmic compression law. The equivalence is established at the level of volumetric compressibility, while the present formulation retains a consistent finite-strain kinematic description.

Bilinear logarithmic compressibility and practical regime. Classical soil models such as Modified Cam–Clay describe the void ratio–effective stress relation using a bilinear logarithmic form, with a recompression slope κ and a virgin compression slope λ,

$$e(\sigma') = \begin{cases} e_0 - \kappa \ln\left(\dfrac{\sigma'}{\sigma'_0}\right), & \sigma' \leq \sigma'_p, \\ e_p - \lambda \ln\left(\dfrac{\sigma'}{\sigma'_p}\right), & \sigma' > \sigma'_p, \end{cases} \tag{61}$$

where σ'_p is the preconsolidation stress and e_p ensures continuity at yield.

In the sedimentation–self-weight consolidation problems considered here, the material is initially deposited at very low effective stress and very high void ratio. As consolidation proceeds, the effective stress increases monotonically under self-weight (and, when applicable, drainage or a vacuum). In practice, the stress state rapidly exceeds the reference stress σ_{ref} and remains in a normally consolidated condition.

Under these conditions, the response is governed predominantly by the virgin compression branch ($\sigma' > \sigma'_p$), which is itself logarithmic in effective stress. The Merkelbach law therefore reproduces the same practical compressibility behavior as the bilinear logarithmic constitutive law as used in complex constitutive law like Modified Cam–Clay formulation, facilitating direct comparison between the two approaches.

Description of the COMSOL benchmark problem. The reference study reported a coupled hydro–mechanical consolidation problem solved with the finite-element implementation available in COMSOL Multiphysics and compared it with a finite-difference large-strain formulation (Li et al., 2025). The configuration consists of a two-dimensional soil column subjected to self-weight, with a partially drained zone at the base representing a prefabricated horizontal drain (PHD) (see Fig. 12). The mechanical response of the soil skeleton in the COMSOL simulations was described using a Modified Cam–Clay model, while pore-water flow was governed by Darcy's law. Large-strain kinematics were activated in order to account for geometric nonlinearity during consolidation. Settlement evolution, pore-pressure dissipation, and void-ratio distributions were reported as the main outputs for comparison. In the reference study, the COMSOL results were used as a benchmark to assess the validity of the finite-difference formulation.

Comparison using the logarithmic void ratio–effective stress relation. To enable a direct comparison with the benchmark results reported in Li et al. (2025), the concentration–stress closure of the present finite-element formulation was reformulated using the same logarithmic void ratio–effective stress relation adopted in the reference study for the comparison case. In the present framework, the constitutive law is written as

$$e = e_0 - k_0 \ln\left(\frac{\sigma' + \sigma_{\mathrm{ref}}}{\sigma'_0 + \sigma_{\mathrm{ref}}}\right), \tag{62}$$

where e_0 is the initial void ratio, k_0 is the compression index, σ'_0 is the reference effective stress, and σ_{ref} is a small regularization stress introduced to avoid singular behavior at very low stress levels. The void ratio is related to the solid volume fraction through

$$e = \frac{1-\phi_s}{\phi_s},$$

so that the logarithmic compressibility law is embedded directly into the ϕ_s-based formulation.

While the kinematics remain fully finite strain, with the volumetric deformation described by the Jacobian $J = \det \mathbf{F}$ and $\varepsilon_v = \ln J$, the constitutive response is expressed through the logarithmic void ratio–stress relation in Eq. (62). This allows the present formulation to recover the same compressibility trend as that used in the benchmark study while keeping the finite-strain transport framework unchanged.

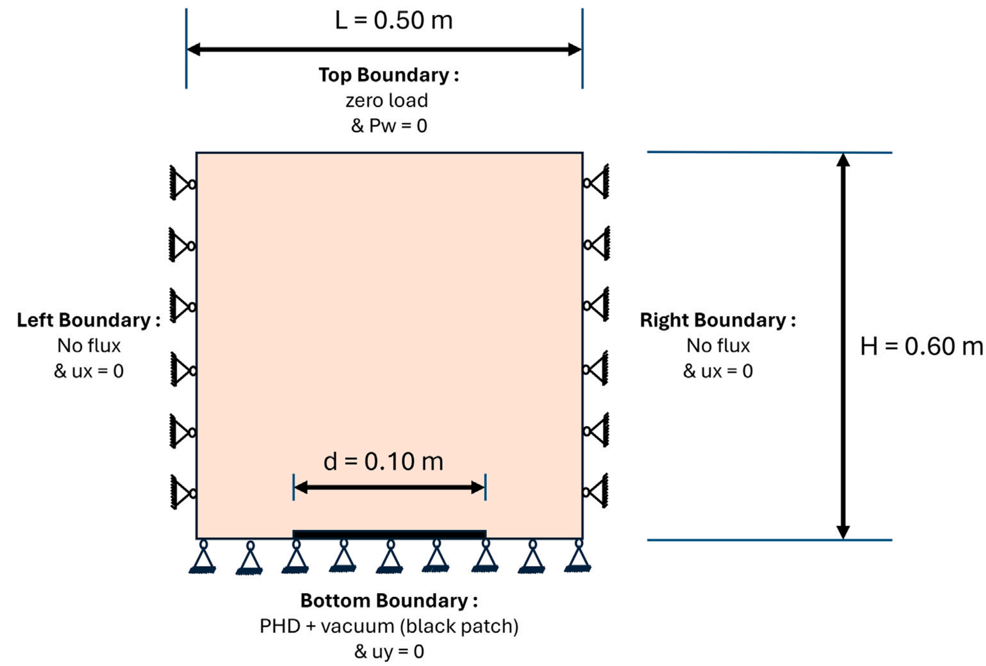

Fig. 12. Comparison between the settlement experimental measurements and the FEM model PHD.

Table 3
Input parameters used in the benchmark comparison.

Parameter	Symbol	Value
Initial void ratio	e_0	5
Reference void ratio	e_0^r	5
Reference effective vertical stress (kPa)	σ_0'	5
Initial horizontal permeability (m/s)	k_{h0}	2.4×10^{-11}
Initial vertical permeability (m/s)	k_{v0}	2.4×10^{-11}
Horizontal permeability exponent	n_h	3.21
Vertical permeability exponent	n_v	3.21

For consistency with the reference study, the following parameters were used: $e_0 = 5.0$, $\sigma_0' = 5$ kPa, $k_{h0} = k_{v0} = 2.4 \times 10^{-11}$ m/s, and $n_h = n_v = 3.21$. The regularization stress was taken as

$$\sigma_{\text{ref}} = 0.0193 \exp(0.3e_0) \text{ kPa},$$

following the expression reported in the reference work (see Table 3). All other model components were kept identical to those used in the previous comparisons.

Equivalent boundary-condition reconstruction in the present model. A difficulty in reproducing the reported COMSOL benchmark lies in the fact that, although the constitutive parameters and drainage layout are clearly specified in Li et al. (2025), the exact drain-state interpretation in the COMSOL comparison is not fully explicit in terms of a directly prescribed local void ratio. In the present model formulation, the drain boundary is therefore introduced through an equivalent bottom value of the solid volume fraction, chosen so as to reproduce the strongly compacted state observed near the drainage strip in the benchmark results.

More specifically, the bottom drain state is related to an equivalent effective stress level obtained by combining the submerged self-weight contribution and an additional drainage-induced stress increase, written here as

$$P_{sk}^{eq} = \phi_0(\rho_s - \rho_w)gH - P_{\text{vac}}, \tag{63}$$

where ϕ_0 is the initial solid fraction, H is the initial column height, and P_{vac} is an equivalent vacuum level. In the present comparison, the value

$$P_{\text{vac}} = -40 \text{ kPa}$$

was adopted because it yields a bottom drain void ratio consistent with the compaction level reported near the drainage strip in the benchmark figure. This value should therefore be interpreted as an equivalent reconstruction adopted in the present model, rather than as a boundary value explicitly prescribed in Li et al. (2025).

Instead of prescribing pore pressure directly, the boundary value of the solid fraction is obtained by inverting the logarithmic compression law,

$$e = e_0 - k_0 \ln\left(\frac{\sigma' + \sigma_{\text{ref}}}{\sigma_0' + \sigma_{\text{ref}}}\right), \qquad \phi = \frac{1}{1+e}.$$

Evaluating this relation at

$$\sigma' = P_{sk}^{eq} + \sigma_0'$$

gives the imposed bottom value

$$\phi^{\text{bot}} = \frac{1}{1 + e_{\text{bot}}},$$

with

$$e_{\text{bot}} = e_0 - k_0 \ln\left(\frac{P_{sk}^{eq} + \sigma_0' + \sigma_{\text{ref}}}{\sigma_0' + \sigma_{\text{ref}}}\right). \tag{64}$$

Hence, in the present formulation the boundary condition is applied directly on the solid volume fraction ϕ_s, but its value is chosen so that the resulting local compaction level remains consistent with the drain-side state observed in the benchmark results. This is therefore an equivalent reconstruction of the benchmark drain condition within the present ϕ_s-based finite-strain framework (see Fig. 13).

Results. Under the present formulation, the predicted void-ratio profiles show a good overall agreement with the benchmark results (see Figs. 14 and 15). The spatial distribution of the void ratio and its evolution in time are well captured, confirming that the use of the logarithmic compressibility law enables the present framework to reproduce the main features of the reference solution.

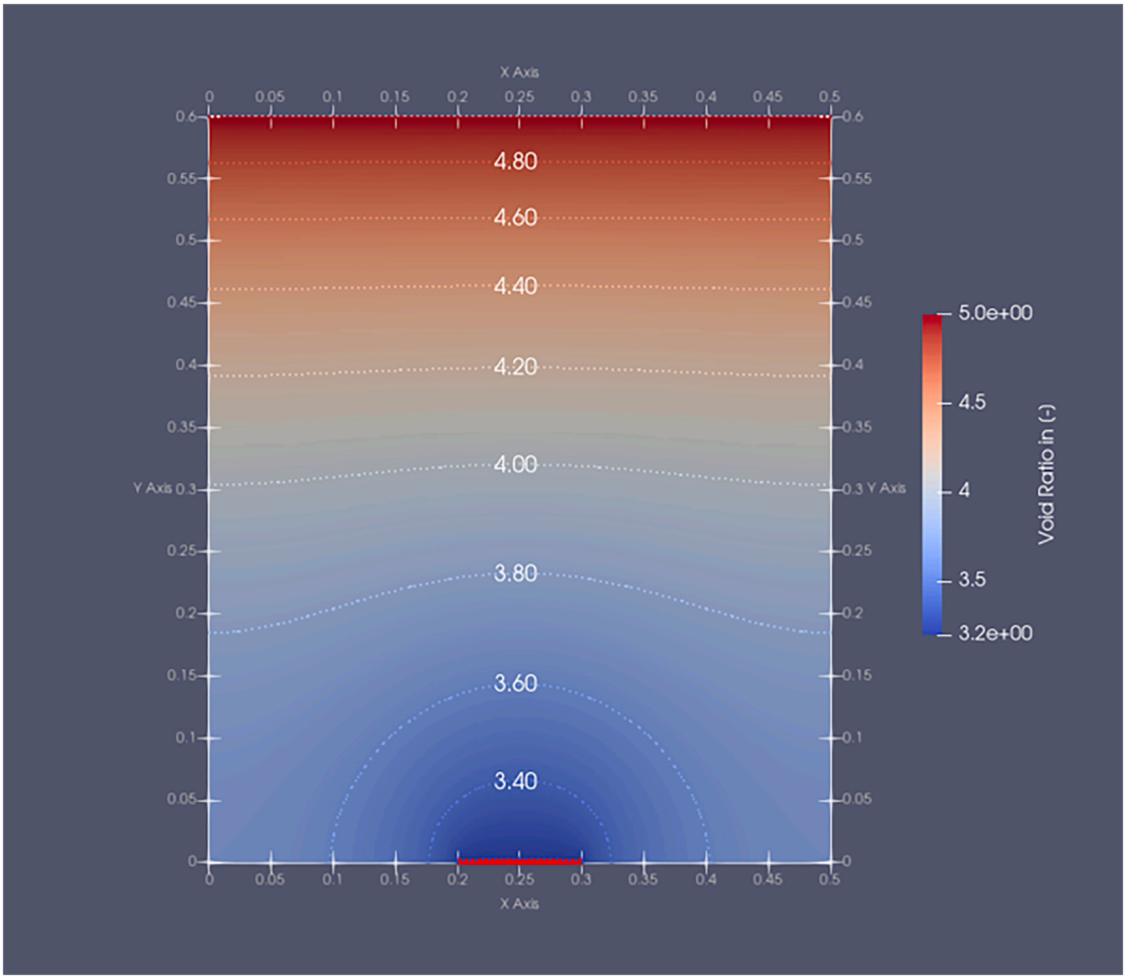

Fig. 13. Spatial distribution of the void ratio obtained from the present finite element model in the PHD case study. The results are visualized in ParaView and illustrate the evolution of the void ratio field under gravity-driven consolidation. The color scale represents the magnitude of the void ratio, while isolines highlight the spatial gradients within the domain.

The remaining differences are primarily localized in the vicinity of the drainage zone. This behavior is consistent with the observations reported in Li et al. (2025), where the strongest gradients and discrepancies are also concentrated near the drainage region. In the present model, this can be attributed to the equivalent reconstruction of the drain boundary condition, which is imposed through a prescribed solid fraction, whereas in the reference study the drainage condition is formulated directly in terms of hydro–mechanical variables.

Away from the drainage zone, the agreement between the present results and the benchmark solution remains very good, indicating that the proposed finite-strain formulation provides a consistent approximation of the void-ratio distribution for the considered configuration.

10. Discussion

10.1. Unified formulation of sedimentation and consolidation

The primary contribution of this work is the demonstration that sedimentation and consolidation can be described within a single, continuous mathematical framework. Although the dominant physical mechanisms differ between these regimes — viscous settling and hindered settling during sedimentation, and effective stress development with Darcy drainage during consolidation — the governing equation preserves the same advection–diffusion structure.

This structural consistency is fundamental. It allows the transition from suspension-like behavior to load-bearing soil behavior to emerge naturally through the concentration dependence of permeability and effective stress, without requiring artificial switching criteria at the gelling point. The evolution of material response is therefore governed by the same transport equation, with smoothly varying coefficients, ensuring both physical continuity and numerical stability.

10.2. Interpretation of the Merkelbach compressibility law

In this work, the Merkelbach stress–concentration relation is used as a macroscopic compressibility closure for very soft sediments undergoing self-weight consolidation. The relation describes how the material stiffens progressively as the solid volume fraction increases during densification. It directly links effective stress to concentration and therefore provides a practical way to capture the evolution from a weak, highly compressible deposit to a denser and stiffer soil.

The Merkelbach law is not an elasto-plastic constitutive model in the classical sense. It does not distinguish between elastic and plastic strains, nor does it introduce a yield surface or hardening rule. Instead, it represents a concentration-dependent compressive-strength relation that is sufficient for gravity-driven, normally consolidated conditions, where the stress state increases monotonically during settlement.

Importantly, in the small-strain limit, the power-law form of the Merkelbach relation becomes equivalent to a standard logarithmic void ratio–effective stress relationship. In this sense, it is consistent with classical consolidation theory when deformations are small, while

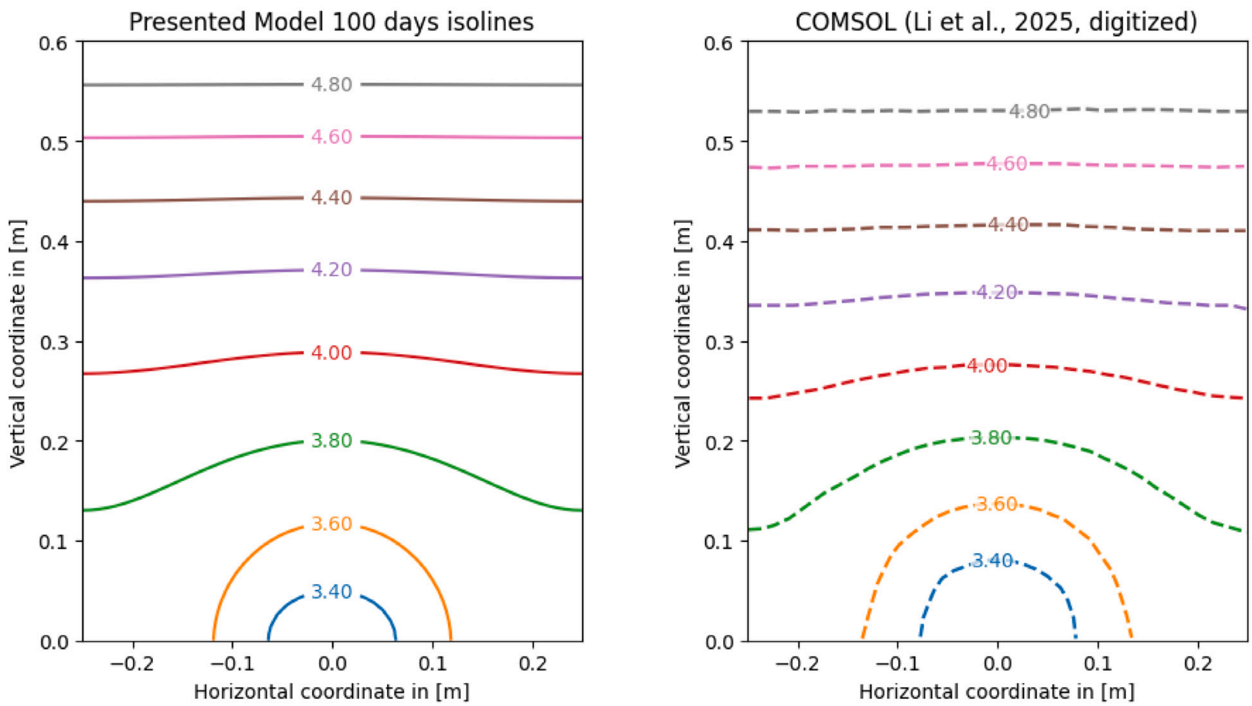

(a) Present model after 100 days (b) COMSOL result digitized from [Li et al., 2025]

Fig. 14. Comparison of the void-ratio distribution at $t = 100$ days under partial PHD arrangement: (a) present model; (b) COMSOL result digitized from Li et al. (2025).

retaining a finite-strain description that remains valid for the large settlements typical of very soft sediments.

Within the scope of the present study — sedimentation and self-weight consolidation dominated by vertical compression — this simplified closure provides a mechanically consistent description of material stiffening without requiring the additional constitutive complexity associated with advanced elasto-plastic models.

10.3. Comparison with logarithmic compressibility

The stress–concentration relation was reformulated using the same logarithmic void ratio–effective stress law adopted in the COMSOL benchmark study. All other model components, including hydraulic parameters, boundary conditions, and finite-strain kinematics, were kept unchanged.

With this logarithmic relation, the present large-strain finite-element formulation reproduces the solid fraction profiles reported in the COMSOL results in a good accuracy despite the simplified hypothesis of the presented model and when also the same constitutive model is used.

The formulation therefore provides a transport-based framework in which either a power-law or a logarithmic stress–concentration relation can be implemented without modifying the governing advection–diffusion structure.

10.4. Large-strain formulation and drainage verification

The governing equations were implemented in a finite-strain framework, where volumetric deformation is described by the Jacobian $J = \det \mathbf{F}$ and the concentration field is solved in the current configuration. This ensures geometric consistency in problems involving significant settlement and reduction of layer thickness. In the limit of small deformations, the formulation reduces to the classical small-strain description.

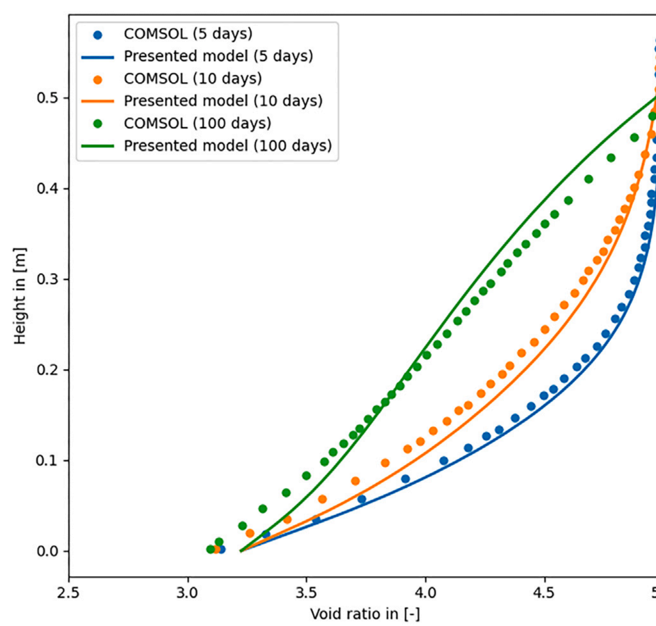

Fig. 15. Comparison of void-ratio profiles along depth at different times for the partial PHD arrangement. The COMSOL curves are digitized from Li et al. (2025).

It should be noted that the simplified nature of the present formulation refers to its constitutive structure rather than to a formal benchmark of computational performance. In contrast to fully coupled finite-strain poromechanical formulations combined with advanced elasto-plastic constitutive models, the present approach avoids tensorial stress updates, return-mapping procedures, and the solution of additional constitutive internal variables. The resulting nonlinear problem therefore involves a simpler constitutive structure while retaining the essential mechanisms governing gravity-driven sedimentation and consolidation.

Drainage conditions were incorporated through flux boundary terms without modifying the governing advection–diffusion equation. The numerical results show the expected acceleration of consolidation and modification of solid fraction profiles when drainage is activated. This confirms that the same transport-based formulation consistently handles both undrained and drained configurations within the range of problems investigated in this study.

10.5. Extension to staged deposition and practical scenarios

An important advantage of the simplified concentration-based framework is its suitability for modeling staged deposition and progressive filling operations. Because the governing equation remains unchanged, additional layers can be introduced by updating the domain geometry and initial concentration field without modifying the underlying transport structure. Similarly, drainage activation can be incorporated through boundary flux conditions within the same formulation.

This flexibility makes the model particularly attractive for large-scale reclamation and sediment management applications, where filling sequences and drainage configurations evolve over time. Typical examples include dewatering fields, land reclamation projects, dredged-material disposal sites, and tailings storage facilities, where large settlements develop under self-weight loading and controlled drainage conditions.

Although the present study focuses on kaolinite K1 and Marker Wadden mud, the governing equations are formulated independently of a specific sediment type. The framework can therefore be applied to other fine-grained soils, including natural clays, silts, and clay–silt mixtures, provided that appropriate constitutive relationships for compressibility, permeability, and sedimentation behavior are available.

10.6. Limitations

The present formulation is specifically tailored to gravity-driven sedimentation and consolidation problems dominated by vertical deformation. Under these conditions, the concentration-based stress law combined with the advection–diffusion structure provides a mechanically consistent description of the evolution from suspension to consolidated soil.

The proposed framework is not restricted to a particular drainage configuration. Complex drainage layouts can be represented through the appropriate specification of hydraulic boundary conditions and material properties. Examples include partially drained boundaries, radial drainage, vertical drains, horizontal drains, and spatially varying drainage fluxes. Consequently, the framework is applicable to a broad range of practical sedimentation and consolidation problems.

However, in cases involving localized mechanical loading — such as foundations, embankments, or strongly non-uniform stress application — the stress state may become significantly non-hydrostatic and substantial shear deformation may develop. In such situations, a fully coupled large-strain poromechanical formulation with tensorial stress representation and explicit elasto-plastic behavior would be required. Similarly, problems involving significant lateral deformation, stress redistribution, or failure mechanisms may exceed the range of validity of the present settlement-dominated formulation.

Another limitation of the present approach is the use of a single solid volume fraction field to describe the sediment. The formulation therefore does not explicitly account for particle-size segregation or differential settling between particle populations. Such effects may become important for highly polydisperse sediments, where the local particle-size distribution evolves during sedimentation and subsequently influences the consolidation response. Extension toward multi-class formulations capable of tracking several particle populations simultaneously remains a topic for future work.

It should be noted that the objective of the present study is to assess the proposed numerical framework rather than to investigate the calibration of the Merckelbach–Kranenburg model parameters. A detailed sensitivity analysis of the parameters D_f, K_σ, and K_k was previously presented by the authors in Myouri and Chassagne (2026). That study showed that different parameter combinations can lead to similar model predictions, highlighting a degree of parameter non-uniqueness. Therefore, the results presented here should be interpreted in the context of the selected parameter set.

The present work is further restricted to fully saturated conditions. Although extensions of Gibson-type formulations to unsaturated sediments have been proposed in the literature, the assumptions adopted in the present framework may no longer remain valid during drying. Unsaturated conditions can induce suction-driven stresses, shrinkage, lateral stress development, and cracking, all of which may strongly affect both the hydraulic and mechanical response of the material. Extending the framework toward drying, unsaturated behavior, and cracking therefore remains an important area for future research.

Furthermore, accurate simulation of multi-stage deposition problems requires careful enforcement of continuity conditions for effective stress and pore pressure across evolving interfaces. While the present framework provides the structural basis for such extensions, a fully interface-consistent implementation is left for future work.

11. Conclusions

This paper presented a unified finite-element model for sedimentation and consolidation of soft clay suspensions. The main idea is that both processes can be described using a single advection–diffusion equation, where the difference between sedimentation and consolidation comes from the constitutive relations and not from different governing equations.

The model was validated using experimental data for kaolinite K1 and Marker Wadden mud. It successfully reproduced interface evolution, density profiles, and the transition from settling to consolidation. The smooth transition around the gelling concentration allowed a stable and physically consistent description of this change in behavior.

In the consolidation regime, the Merkelbach compressive-strength law was sufficient to predict the mechanical response of the soil. When the compressibility law was replaced by a logarithmic Modified Cam–Clay relation, the results matched the COMSOL benchmark. This shows that differences between models are mainly due to the assumed compressibility law, not due to the large-strain formulation or the numerical method.

Drainage conditions, including localized drainage and vacuum loading, were also verified. The formulation correctly captured accelerated consolidation and redistribution of the solid fraction, demonstrating that the simplified approach remains valid under practical boundary conditions.

Overall, the proposed framework provides a clear and efficient way to model very soft sediments from suspension to consolidated soil. It keeps the essential physics of gravity-driven settlement while remaining compatible with large deformations.

Future work will focus on staged deposition and more complex loading conditions, where full hydro-mechanical coupling may be required like in the case of localized loading and the unsaturation of soft material.

Notation

Throughout this work, a Lagrangian description is adopted unless otherwise stated. Bold lowercase symbols denote vectors, bold uppercase symbols denote second-order tensors, and standard symbols denote scalar quantities.

ϕ_s	Solid volume fraction
ϕ_w	Water volume fraction
ϕ_0	Reference solid volume fraction
ϕ_{gel}	Gelling concentration
p_w	Pore-water pressure
p_e	Excess pore-water pressure ($p_e = p_w - p_{\mathrm{hyd}}$)
σ_{sk}	Scalar effective stress (positive in compression)
$C(\phi_s)$	Compressibility term

D_0	Brownian diffusion coefficient
k_B	Boltzmann constant
T	Absolute temperature
ρ_s, ρ_w	Solid and water densities
g	Gravitational acceleration magnitude
z	Elevation coordinate
α	Transition sharpness parameter

$\mathbf{x}$	Current (Eulerian) position
$\mathbf{X}$	Reference (Lagrangian) position
$\mathbf{u}$	Displacement vector ($\mathbf{u} = \mathbf{x} - \mathbf{X}$)
$\mathbf{v}_0$	Stokes settling velocity
$\mathbf{g}$	Gravitational acceleration vector
$\mathbf{q}_w$	Water flux in current configuration
$\mathbf{J}_{w/s}$	Water flux relative to solid skeleton
$\mathbf{V}_{\mathrm{adv}}$	Advective velocity
$\mathbf{n}$	Outward unit normal vector

$\mathbf{F}$	Deformation gradient
$J = \det(\mathbf{F})$	Jacobian of deformation
$\mathbf{K}_w$	Hydraulic conductivity tensor
$\mathbf{D}_{\mathrm{diff}}$	Diffusion tensor
$\boldsymbol{\sigma}$	Total Cauchy stress tensor
$\boldsymbol{\sigma}_{sk}$	Effective stress tensor
$\mathbf{I}$	Identity tensor

$\mathrm{grad}_{\mathbf{x}}$	Gradient in current configuration
$\mathrm{Grad}_{\mathbf{X}}$	Gradient in reference configuration
$\mathrm{div}_{\mathbf{x}}$	Divergence in current configuration
$\mathrm{Div}_{\mathbf{X}}$	Divergence in reference configuration
$\frac{D}{Dt}$	Material derivative (following the solid phase)

Ω_0	Reference domain
$\partial\Omega_0$	Boundary of the domain
Γ_{top}	Top boundary
Γ_{imp}	Impermeable boundary
Γ_{drain}	Drainage boundary

CRediT authorship contribution statement

Ismail Myouri: Writing – original draft, Visualization, Validation, Software, Methodology, Investigation, Formal analysis, Data curation, Conceptualization. **Claire Chassagne:** Writing – review & editing, Validation, Supervision, Resources, Project administration, Methodology, Investigation, Funding acquisition, Formal analysis, Conceptualization.

Funding declaration

This work was carried out within the Sediment-to-Soil (S2S) project and was supported by the Dutch Research Council (NWO) under the Open Technology Programme, grant number 2020-II TTW (2021/TTW/01144384).

Declaration of competing interest

The authors declare that they have no known competing financial interests or personal relationships that could have appeared to influence the work reported in this paper.

Acknowledgments

The authors gratefully acknowledge the TU Delft MUDNET community for their support and the productive discussions throughout the project.

Appendix A. Supplementary data

Supplementary material related to this article can be found online at https://doi.org/10.1016/j.compgeo.2026.108407.

Data availability

The data supporting the findings of this study are included within the article and its supplementary material.

References

Barciela-Rial, M., et al., 2024a. Experimental and numerical analysis of underwater consolidation of dredged sediment: a case of study for the marker wadden. Front. Mar. Sci..

Barciela-Rial, M., et al., 2024b. Sediment behavior in marker wadden reclamation. Front. Mar. Sci..

Barron, R.A., 1948. Consolidation of fine-grained soils by drain wells. Trans. Am. Soc. Civ. Eng. 113, 718–742.

Been, K., Sills, G., 1981. Self-weight consolidation of soft soils: an experimental and theoretical study. Geotechnique 31 (4), 519–535.

Biot, M.A., 1941. General theory of three-dimensional consolidation. J. Appl. Phys. 12 (2), 155–164.

Biot, M.A., 1955. Theory of elasticity and consolidation for a porous anisotropic solid. J. Appl. Phys. 26 (2), 182–185.

Borja, R.I., Alarcón, E., 1995. A mathematical framework for finite strain elastoplastic consolidation. part 1: Balance laws, variational formulation and linearization. Comput. Methods Appl. Mech. Engrg. 122 (1–2), 145–171.

Borja, R.I., Tamagnini, C., Alarcón, E., 1998a. Elastoplastic consolidation at finite strain. Comput. Methods Appl. Mech. Engrg. 159 (1–2), 103–122.

Borja, R.I., Tamagnini, C., Alarcón, E., 1998b. Elastoplastic consolidation at finite strain. Part 2: Finite element implementation and numerical examples. Comput. Methods Appl. Mech. Engrg. 159 (1–2), 103–122.

Brooks, A.N., Hughes, T.J.R., 1982. Streamline upwind/Petrov–Galerkin formulations for convection dominated flows with particular emphasis on the incompressible Navier–Stokes equations. Comput. Methods Appl. Mech. Engrg. 32 (1–3), 199–259.

Buscall, R., 1990. The sedimentation of concentrated colloidal suspensions. Colloids Surf. 43, 33–53.

Carnahan, N.F., Starling, K.E., 1969. Equation of state for nonattracting rigid spheres. J. Chem. Phys. 51 (2), 635–636.

Chassagne, C., 2019. Understanding the natural consolidation of slurries using colloid science. In: 17th European Conference on Soil Mechanics and Geotechnical Engineering, ECSMGE 2019. International Society for Soil Mechanics and Geotechnical Engineering, pp. 1–8.

Chassagne, C., 2021. Introduction to colloid science: Applications to sediment characterization.

Chu, J., Varaksin, S., 2000. Soil improvement and ground modification methods.

Darcy, H., 1856. Les fontaines publiques de la ville de Dijon. Dalmont, Paris.

Ern, A., Guermond, J., 2004. Theory and Practice of Finite Elements. Springer.

Geng, X., Yu, H.S., 2017. A large-strain radial consolidation theory for soft clays improved by vertical drains. Geotechnique 67 (11), 1020–1028.

Gibson, R.E., MJL, G., 1967. The theory of one-dimensional consolidation of saturated clays: 1. finite non-linear consolidation of thin homogeneous layers. Geotechnique 17 (3), 261–273.

Gibson, R.E., Schiffman, R.L., Cargill, K.W., 1981. The theory of one-dimensional consolidation of saturated clays: Ii. finite nonlinear consolidation of thick homogeneous layers. Can. Geotech. J. 18 (2), 280–293.

Hansbo, S., 1981. Consolidation of fine-grained soils by prefabricated drains. In: Proceedings of the 10th International Conference on Soil Mechanics and Foundation Engineering. vol. 3, pp. 677–682.

Hol, N.J., Myouri, I., Chassagne, C., Pel, L., 2025a. Determination of the surface relaxivity of soft sediment using particle size and shape. J. Magn. Reson. Open 100198.

Hol, N.J., Pel, L., Kurvers, M., Chassagne, C., 2025b. Fast 1D NMR imaging of clay sedimentation using a multi-slice stepper motor method. Exp. Fluids 66 (1), 9.

Hughes, T., 2012. The Finite Element Method: Linear Static and Dynamic Finite Element Analysis. Dover.

Indraratna, B., Zhong, R., Fox, P.J., Rujikiatkamjorn, C., 2017. Large-strain vacuum-assisted consolidation with non-darcian radial flow incorporating varying permeability and compressibility. J. Geotech. Geoenvironmental Eng. 143 (1), 04016088.

Kynch, G.J., 1952. A theory of sedimentation. Trans. Faraday Soc. 48, 166–176.

Li, P.-L., Song, D.-B., Yin, Z.-Y., Yin, J.-H., 2025. Large strain consolidation model for very soft soils with prefabricated horizontal drains considering nonlinear compression and creep. Acta Geotech. 20, 1431–1453.

Merckelbach, Kranenburg, Winterwerp, J., 2002. Strength modelling of consolidating mud beds. In: Proceedings in Marine Science. vol. 5, Elsevier, pp. 359–373.

Mesri, G., Olson, R.E., 1997. Consolidation characteristics of soils. Géotechnique 47 (4), 747–756.

Miedema, S.A., 2006. Slurry transport: Fundamentals, a historical overview and the delft head loss and limit deposit velocity framework.

Moseley, M.P., Kirsch, K., 2004. Ground improvement.

Myouri, I., Chassagne, C., 2026. Self-weight consolidation of kaolinite suspensions measured by nuclear magnetic resonance: experiments and large-strain modeling. Preprint, available on SSRN; under review in Computers and Geotechnics.

Myouri, I., Hol, N., Pel, L., Chassagne, C., 2025. Self-weight consolidation of kaolinite suspensions in deionized water measured by nuclear magnetic resonance – experiments and modelling. Manuscript under review at Computers and Geotechnics.

Pane, V., Schiffman, R.L., 1985. A note on sedimentation and consolidation. Géotechnique 35 (1), 69–72.

Rial, M.B., 2019. Consolidation and drying of slurries: A building with nature study for the marker wadden.

Richardson, J., Zaki, W., 1997. Sedimentation and fluidisation: Part i. Chem. Eng. Res. Des. 75, S82–S100.

Russel, W.B., Saville, D.A., Schowalter, W.R., 1991. Colloidal Dispersions. Cambridge University Press.

Terzaghi, K., 1925. Erdbaumechanik auf bodenphysikalischer Grundlage. F. Deuticke.

Tian, H., Wang, Y., 2023. Data-driven and physics-informed Bayesian learning of spatiotemporally varying consolidation settlement from sparse site investigation and settlement monitoring data. Comput. Geotech. 157, 105328.

Tian, H., Wang, Y., Zhang, D., 2025. Real-time model updating and prediction of three-dimensional time-varying consolidation settlement using machine learning. J. Rock Mech. Geotech. Eng. 17 (9), 5954–5969.

Toorman, E.A., 1996. Sedimentation and self-weight consolidation: General unifying theory. Géotechnique 46 (1), 103–113.

Van Rijn, L.C., 2019. Land Reclamation Using Dredged Mud. Technical report.

Winterwerp, J.C., 2002. On the flocculation and settling velocity of cohesive sediment. Cont. Shelf Res. 22, 1339–1360.

Zienkiewicz, O., Taylor, R., Zhu, J., 2013. The Finite Element Method: Its Basis and Fundamentals. Elsevier.